

# Optically-Selected BLR-less Active Galactic Nuclei from the SDSS Stripe82 Database I: The Sample

Xue-Guang Zhang<sup>1,2</sup>

<sup>1</sup>*Purple Mountain Observatory, Chinese Academy of Sciences, 2 Beijing XiLu, NanJing, JiangSu, 210008, P. R. China*

<sup>2</sup>*Chinese Center for Antarctic Astronomy, NanJing, JiangSu, 210008, P. R. China*

## ABSTRACT

This is the first paper in a dedicated series to study the properties of the optically selected BLR-less AGNs (Active Galactic Nuclei with no-hidden central broad emission line regions). We carried out a systematic search for the BLR-less AGNs through the Sloan Digital Sky Survey Legacy Survey (SDSS Stripe82 Database). Based on the spectral decomposition results for all the 136676 spectroscopic objects (galaxies and QSOs) with redshift less than 0.35 covered by the SDSS Stripe82 region, our spectroscopic sample for the BLR-less AGNs includes 22693 pure narrow line objects without broad emission lines but with apparent AGN continuum emission  $R_{AGN} > 0.3$  and apparent stellar lights  $R_{ssp} > 0.3$ . Then, using the properties of the photometry magnitude RMS ( $RMS$ ) and the Pearson's coefficients ( $R_{1,2}$ ) between two different SDSS band light curves:  $RMS_k > 3 \times RMS_{M_k}$  and  $R_{1,2} > \sim 0.8$ , the final 281 pure narrow objects with true photometry variabilities are our selected reliable candidates for the BLR-less AGNs. The selected candidates with higher confidence levels not only have the expected spectral features of the BLR-less AGNs, but also show significant true photometry variabilities. The reported sample at least four-times enlarges the current sample of the BLR-less AGNs, and will provide more reliable information to explain the lack of the BLRs of AGNs in our following studies.

**Key words:** Galaxies:Active – Galaxies:nuclei – Galaxies:Seyfert – QSOs:Emission lines

## 1 INTRODUCTION

For Active Galactic Nuclei (AGN), the well-known constantly being revised Unified Model (Rees 1984; Miller & Goodrich 1990; Antonucci 1993; Urry & Padovani 1995; Zhang & Wang 2006; Seymour et al. 2007; Wang & Zhang 2007; Hiner et al. 2009; Smolcic & Riechers 2011; Elitzur 2012; Marinucci et al. 2012; Malizia et al. 2012), more recent review can be found in Bianchi et al. (2012) can be applied to explain most of the different observed phenomena of different kinds of AGN, due to the different orientation angles of the central accretion disk combining with the different central accretion rates, the different covering factors of the dust torus etc.. Based on the Unified Model, one simple viewpoint is that type 2 AGN (no broad emission lines in observed spectra) are intrinsically like type 1 AGN (apparent broad lines in observed spectra), but their broad-line regions (BLRs) are hidden from our view by the dust torus and/or high density dust clouds. This simple viewpoint can be strongly supported by the clearly detected polarized broad emission lines and/or by the clearly detected broad infrared broad emission lines for some type 2 AGN (Miller & Goodrich

1990; Axon et al. 1994; Kay 1994; Young et al. 1996; Heisler et al. 1997; Veilleux et al. 1997; Hiner et al. 2009; Young et al. 1998; Barth et al. 1999a,b; Veilleux et al. 1999; Awaki et al. 2000; Moran et al. 2000; Lutz et al. 2000; Tran 2001; Schmidt et al. 2002; Tran 2003; Nagao et al. 2004).

However, the increasing number of studies, especially on the analysis of the X-ray band characters and the analysis on the polarimetric spectral properties for some type 2 objects, have shown that besides the type 1 AGN (including those seriously obscured objects, such as type 1.5, type 1.9 AGN etc.) and the type 2 AGN, there is one special kind of AGN, BLR-less AGN (named as true type 2 AGN or AGN without hidden BLRs in some references): AGN without central BLRs (Panessa & Bassani 2002; Laor 2003; Georgantopoulos & Zezas 2003; Hawkins 2004; Ghosh et al. 2007; Bianchi et al. 2008; Brightman & Nandra 2008; Shi et al. 2010; Malizia et al. 2012; Petrov & Yankulova 2012). Based on the polarimetric spectral features and/or based on the photometric magnitude variabilities, around 70 BLR-less AGNs have been reported and discussed in the literature. Besides the contributions to improve the Unified Model for AGN, a study the properties of the BLR-less AGNs should provide more information on the for-

mation (or the suppression) of the BLR of AGN, and/or additional information about transition stages of the accretion etc. (Laor 2003; Nicastro et al. 2003; Wolter et al. 2005; Shemmer et al. 2006; Gliozzi et al. 2007; Hawkins 2007; Elitzur & Ho 2009; Panessa et al. 2009; Cao 2010; Gliozzi et al. 2010; Plotkin et al. 2010; Shi et al. 2010; Tran et al. 2011; Marinucci et al. 2012; Petrov & Yankulova 2012).

So far, there have been several methods proposed to explain the BLR absence in AGNs. Based on the spectropolarimetric sample from Tran (2001), Nicastro et al. (2003) have shown that the absence or presence of the hidden BLR in the type 2 AGNs is controlled by the central accretion, under the assumption that the BLRs are formed by the accretion disk instabilities occurring around the critical radius at which the gas pressure dominated accretion disk changes to being dominated by the radiation pressure (Nicastro 2000). Laor (2003) have shown that BLR can not be able to survive, if central luminosity is much lower. Elitzur & Ho (2009) have shown that the disk-wind scenario for BLR and torus obscuration predicts the disappearance of the BLR for AGNs at low luminosities. More recently, Cao (2010) have shown that for the low luminosity AGNs containing ADAF, the inner small cold disk is evaporated completely and the outer thin accretion disk may be seriously suppressed, which leads to the lack of the BLR. However, based on the study of the current sample of the BLR-less AGNs, the reason of the BLR absence in BLR-less AGN is still controversial. Marinucci et al. (2012); Petrov & Yankulova (2012) supported the model proposed by Nicastro et al. (2003), through a sample of 18 BLR-less AGNs (Marinucci et al. 2012) and a sample of 36 BLR-less AGNs (Petrov & Yankulova 2012). Zhang & Wang (2006) have found that the BLR absence in the BLR-less AGNs is probably caused by the less massive black holes and the high accretion rates similar to those in Narrow Line Seyfert I objects, through a sample of 46 BLR-less AGNs. Wang & Zhang (2007) have shown that the lack of BLR could be probably caused by low gas-to-dust ratios, through a sample of 69 BLR-less AGNs. Bian & Gu (2007) have shown that the AGN luminosity plays a major role in the BLR absence in the BLR-less AGNs, while for the high-luminosity BLR-less AGNs, the BLR absence depends not only on the AGN activity, but also on the torus obscuration, through a sample of 49 BLR-less AGNs. Wu & Zhang (2011) have shown that the BLR absence in the luminous BLR-less AGNs depends on the obscuration, however, the BLR absence the less luminous BLR-less AGNs depends on the very low Eddington ratio rather than the obscuration, based on a sample of 71 BLR-less AGNs. Yu & Hwang (2011) have shown that in order to explain the nitrogen overabundance for the BLR-less AGNs, there should be apparent effects from stellar evolution, based on a sample of 33 BLR-less AGNs.

Due to the current small sample of the BLR-less AGNs reported in the literature, some contradictory statements about the properties of the BLR-less AGNs have been reported, which arise mainly due to the limited size of the current sample of the BLR-less AGNs and/or due to the different methods to select the candidates for the BLR-less AGNs. Thus, in this manuscript, we increase the current sample of the BLR-less AGNs. It is clear that

the most direct method to select the BLR-less AGNs is through the polarimetric spectral properties (such as the sample in Tran 2001), and through the continuum variabilities of the pure narrow line objects (such as the sample in Hawkins 2004). Fortunately, the Sloan Digital Sky Survey (SDSS, York et al. 2000; Adelman-McCarthy et al. 2008; Abazajian et al. 2009; Aihara et al. 2011) Stripe82 database, covering the region with the right ascension from 20.7h to 3.3h and with the declination from -1.26 to 1.26, provides an idea to collect the BLR-less AGNs through the properties of the SDSS spectra and the photometric variabilities.

The manuscript is organized as follows. In Section 2, we describe our procedures to collect the candidates for the BLR-less AGNs, based on both the SDSS spectral features and the properties of the photometry variabilities through the SDSS Stripe82 database. Then, our discussions, conclusions and our simple and basic results about the primary parameters of our BLR-less AGNs are shown in the Section 3. The cosmological parameters  $H_0 = 70\text{km} \cdot \text{s}^{-1}\text{Mpc}^{-1}$ ,  $\Omega_\Lambda = 0.7$  and  $\Omega_m = 0.3$  have been adopted.

## 2 DATA SAMPLE FOR BLR-LESS AGNS

In order to select the reliable candidates for the BLR-less AGNs through both the photometry variabilities and the observed spectral features, we applies the following procedures to the objects in the SDSS Stripe82 Database. The emission line parameters should be firstly determined, in order to confirm that our spectroscopic sample includes the pure narrow line objects only (type 2 objects, the objects having both strong and weak broad lines can not be considered). Then, the SDSS photometric light curves of the objects in the spectroscopic sample should be carefully analysed to find the reliable candidates for the BLR-less AGNs.

### 2.1 Line Parameters for the Spectroscopic Objects in the SDSS Stripe82 Region

The SDSS Stripe82 region consists of two scan regions referred to as the north and the south strips. Both the north and the south strips have been repeatedly imaged since 1998. A brief description of the Stripe82 data and coadd can be found in Abazajian et al. (2009). Some detailed descriptions about the constructions for the corrected photometric light-motion curves for the objects in the Stripe82 region can be found in Vidrih et al. (2007), Ivezić et al. (2007), Bramich et al. (2008) and the references therein. Using the properties of the photometric light curves of the spectroscopic objects in the Stripe82 region, we are coming to find the reliable candidates for the BLR-less AGNs.

Because the line parameters (especially, line width and line flux) are necessary for us to create our spectroscopic sample for the BLR-less AGNs: only pure narrow line objects with high quality SDSS spectra are considered in our spectroscopic sample. The following two data files have been collected from the SDSS website ([http://www.sdss3.org/dr8/spectro/spectro\\_access.php](http://www.sdss3.org/dr8/spectro/spectro_access.php)): 'specObj-dr8.fits' which provides the information about the redshifts, the classifications, the positions etc. for all the SDSS spectroscopic objects in the SDSS DR8, and

'galSpecIndx-dr8.fits' which provides the information about the line parameters for all the SDSS spectroscopic objects in the SDSS DR8. Then based on the information of the RA and the DEC for all the objects in the SDSS DR8:  $300 < RA < 60$  and  $-1.25 < DEC < 1.25$ , 229318 SDSS spectroscopic objects with redshift less than 0.35 covered by the Stripe82 region are firstly selected. Here, the restriction on the redshift is applied to ensure the spectra of the collected objects cover both H $\alpha$  and H $\beta$ , in order to check whether there are broad lines. Based on the SDSS pipeline, there are 114788 of 229318 objects classified as 'GALAXY', 92642 of 229318 objects classified as 'STAR' and 21888 of 229318 objects classified as 'QSO'.

Then, by the selected 229318 spectroscopic objects covered in the Stripe82 region, it is straightforward to create our spectroscopic sample including the pure narrow line objects, based on the measured line parameters for all the objects except the stars covered by the Stripe82 region. Due to the contributions from the stellar lights, the spectral decomposition should be firstly applied. In other words, before to measure the line parameters of the emission lines, the contributions of the stars to the SDSS spectrum should be subtracted. Here, the most commonly accepted "Simple Stellar Population" (SSP) method is applied: the stellar contributions in the observed SDSS spectrum can be best fitted and subtracted by the linear combination of the SSPs. The SSP method provides the fundamental link between theory/models and observations:

$$P_{O,\lambda} = \left( \sum_{j=1}^{39} A_j \times P_{ssp,\delta\lambda,r_\lambda} \right) \otimes G(\lambda, \sigma) + P_{AGN,r_\lambda} \quad (1)$$

where  $P_{O,\lambda}$  represents the observed spectrum,  $\delta\lambda$  represents one small wavelength shift between the observed spectrum and the SSPs,  $r_\lambda$  represents one intrinsic reddening factor,  $P_{AGN,r_\lambda}$  represents the AGN component (commonly described by one power-law function) with the reddening factor  $r_\lambda$ ,  $P_{ssp,\delta\lambda,r_\lambda}$  means the SSP components with the wavelength shift  $\delta\lambda$  and with the reddening factor  $r_\lambda$ ,  $G(\lambda, \sigma)$  means one broadening function with the broadening velocity  $\sigma$  (commonly, the stellar velocity dispersion).

Here, we exploit the 39 simple stellar population templates from the Bruzual & Charlot (2003), which include the population age from 5 Myr to 12 Gyr, with three solar metallicities ( $Z = 0.008, 0.05, 0.02$ ). As the detailed discussion in Bruzual & Charlot (2003), the 39 templates can be used to well-describe the characters of nearly all the galaxies in SDSS, such as the distributions of the stellar masses, ages, metallicities etc.. Then through the Levenberg-Marquardt least-squares minimization method applied for the SDSS spectra with the emission lines being masked, the stellar component and the AGN power law continuum component in the SDSS spectra can be clearly determined and separated. A detailed descriptions of the SSP method can be found in Bruzual & Charlot (2003); Kauffmann et al. (2003); Brinchmann et al. (2004); Cid Fernandes et al. (2004); Tremonti et al. (2004); Cid Fernandes et al. (2005b,a); Stasinska et al. (2006); Cid Fernandes et al. (2007); Richards et al. (2009); Vazdekis et al. (2010); Giraud et al. (2011); Maraston & Stromback (2011); Peacock et al. (2011); Bae et al. (2012); Conroy & van Dokkum (2012); Cappellari (2012) etc.. There are several other methods

than SSP used for the spectral decomposition, such as the PCA (Principle Component Analysis) method (Yip et al. 2004; Hao et al. 2005; Li et al. 2005; Vanden Berk et al. 2006; Zhang et al. 2008), ICA (Independent Component Analysis) method (Zhang & Wang 2006). Each method has its own advantages and disadvantages. Here, the SSP method is used, because the SSP method results can provide the direct stellar properties, and moreover the SSP templates can be conveniently collected from the literature. Some examples for the spectral decomposition can be found in Figure 1. From the results shown in the figure, it is clear that both the stellar components and the power law continuum component can be clearly subtracted from the observed SDSS spectrum. The four objects shown in the figure are four reliable candidates in our final sample of the candidates for the BLR-less AGNs.

Once the stellar components are subtracted out, the emission lines can be measured. Here, we mainly focus on the emission lines around the H $\alpha$  and the H $\beta$ , including the optical Fe II emission lines, the broad He II  $\lambda 4687\text{\AA}$  line, the common/extended [O III]  $\lambda 4959, 5007\text{\AA}$  doublet, the narrow/broad H $\beta$ , the [O I]  $\lambda 6300, 6363\text{\AA}$  doublet, the [N II]  $\lambda 6548, 6583\text{\AA}$  doublet, the [S II]  $\lambda 6716, 6731\text{\AA}$  doublet and the narrow/broad H $\alpha$ . Here, the narrow/broad H $\gamma$  and H $\delta$  lines are not considered, due to their weakness, which have no effects on our following results.

It is straightforward to measure the line parameters by simple Gaussian functions applied to the emission lines combined with one power law function used for the AGN continuum, after the subtraction of the stellar contributions. Each narrow Gaussian function (full-width at half maximum less than 800km/s) is applied for each narrow emission line, except the extended components of the [O III]  $\lambda 4959, 5007\text{\AA}$  doublet. For the [O III] doublet, besides the normal narrow gaussian functions, there are two broad gaussian functions applied for the extended wings of the doublet as discussed in Green & Ho (2005). For the doublets [O III] and [N II], the center wavelength ratio, flux ratio and width ratio are fixed to the theoretical values. For the doublets [O I] and [S II], only the center wavelength ratio and the width ratio are fixed to the theoretical values. Two broad gaussian functions (full-width at half maximum larger than 600km/s) are applied for the broad H $\alpha$  (H $\beta$ ), i.e., one normal broad function and one much extended broad function. A simple broad gaussian function is sufficient to describe observed broad H $\alpha$  (H $\beta$ ) of a part of the objects. The main reason to describe the broad Balmer lines by two broad gaussian functions is only to find more better description for the broad line profile, in order to reject the objects with probable broad balmer lines. To further discuss why two broad components are much preferred for some objects are beyond the scope of the manuscript. Then, one broadened Fe II template spectra is applied for the probable Fe II components within the wavelength range from 4100 $\text{\AA}$  to 5600 $\text{\AA}$  (Boroson & Green 1992; Sigut & Pradhan 2003; Kovacevic et al. 2010). Here, the method described in Kovacevic et al. (2010) is applied to measure the Fe II properties. Finally, using the Levenberg-Marquardt least-squares minimization method, the line parameters (including the Fe II) and the characters of the AGN continuum emission can be determined.

Then, based on the measured line parameters:  $P \geq 3 \times P_{err}$  (where  $P$  and  $P_{err}$  represent the measured line

parameters and the correspond uncertainties), among the 136676 objects (114788 objects classified as 'GALAXY' and 21888 objects classified as 'QSO', through the SDSS pipeline), 27806 pure narrow objects (67 of 21888 'QSO' objects and 27739 of 114788 'GALAXY' objects) have apparent and strong narrow emission lines of [O III] and [N II] doublets, but no broad emission lines. Moreover, there are 60066 objects (394 of 21888 QSOs and 59672 of 114788 Galaxies) having much weaker narrow emission lines and no broad lines. For the objects with no broad, the parameter 'subclass' listed in the SDSS data file 'specObj-dr8.fits' is considered, only the objects with the spectroscopic subclassification not including 'BROADLINE' are considered. Finally, the total 87872 objects (27806 pure narrow line objects, and 60066 objects with much weaker narrow lines and no broad lines) are taken up of our first sample. Then, simple classification for the 87872 objects can be done through the well-known BPT diagram (Baldwin, Phillips & Terlevich 1981; Veilleux & Osterbrock 1987; Kewley et al. 2001; Kauffmann et al. 2003; Kewley et al. 2006). There are 17123 objects classified as AGNs (Seyfert galaxies and LINERs), 23144 objects classified as HII galaxies, and 47605 objects not classified due to the less information of narrow line ratios. Figure 2 shows the properties of the objects with strong narrow lines in the BPT diagram. If strong narrow lines are apparent, the commonly used line ratios of [O III]/H $\beta$  and [N II]/H $\alpha$  are used for the classification. If only one line ratio is available, the AGN classification can be done by [O III]/H $\beta$  larger than 10 (or [N II]/H $\alpha$  larger than 1).

There are two more points we should note. On the one hand, although the SDSS standard pipeline output has been used to classify the objects into GALAXY and QSO, some objects classified as GALAXY have apparent broad lines, and some objects classified as QSO have apparent stellar components. Hence, the spectral decomposition is applied to all the spectroscopic objects (galaxies and QSOs) observed in the Stripe82 region. On the other hand, when the BPT diagram is used for the classification, the line ratios of [O III]/H $\beta$  and [N II]/H $\alpha$  are mainly considered. The other line ratios, such as [O II]/H $\beta$  and [S II]/H $\alpha$  are not considered, due to the weak line intensities and/or large effects from the extinction on the line ratios.

## 2.2 Spectroscopic Candidates for the BLR-less AGNs

Our spectroscopic candidates are expected to have the spectral features of the BLR-less AGNs, which are no broad emission lines but apparent power law continuum emission. Here, the spectral decomposition results are discussed for the pure narrow line objects with strong AGN continuum emissions.

First, we check the linear correlation between the AGN continuum luminosity and the broad line luminosity reported by Greene & Ho (2005) for pure QSOs, in order to confirm that we reliably measured AGN continuum luminosities. Figure 3 shows the correlation for the 815 pure type 1 AGNs of which spectra include both apparent broad balmer lines and apparent stellar lights in the Stripe82 region. The main reason for not considering the obscured broad line AGNs (having broad H $\alpha$  but much weak broad H $\beta$ ) is to avoid the effects of the internal extinctions. The

luminosity of the broad H $\beta$  is the total luminosity, in spite of the broad H $\beta$  being described by one or two broad gaussian components. The strong linear correlation is present: the spearman rank correlation coefficient 0.82 with  $P_{null} \sim 0$ . Including the uncertainties in both coordinates, the linear correlation can be written as,

$$\log\left(\frac{L(H\beta)}{\text{erg/s}}\right) = (-13.79 \pm 0.34) + (1.26 \pm 0.007) \times \log\left(\frac{L(5100\text{\AA})}{\text{erg/s}}\right) \quad (2)$$

The result is comparable to the one in Greene & Ho (2005), and indicates our spectral decomposition results are reliable. The right panel of the Figure 3 shows the strong luminosity correlation between the broad H $\alpha$  and the broad H $\beta$  for the 815 pure type 1 AGNs, which will indicate whether our measured line parameters are reliable. The correlation coefficient is about 0.87 with  $P_{null} \sim 0$ . The best fitted result for the luminosity correlation is  $L(H\alpha) = (3.8 \pm 0.1) \times L(H\beta)$ , which indicates small internal extinction for the results in the left panel of Figure 3.

Based on the spectral decomposition results, the following three criteria are used to select for the pure narrow line objects as our spectroscopic candidates for the NLR-less AGNs,

$$\begin{aligned} R_{AGN} &> 30\% \\ R_{ssp} &> 30\% \\ P_{line} &> 3 \times P_{line, err} \end{aligned} \quad (3)$$

where  $R_{ssp} = \frac{f(ssp, 5100\text{\AA})}{f(ssp, 5100\text{\AA}) + f(AGN, 5100\text{\AA})}$  and  $R_{AGN} = \frac{f(AGN, 5100\text{\AA})}{f(ssp, 5100\text{\AA}) + f(AGN, 5100\text{\AA})}$  mean the contributions to the continuum at 5100 $\text{\AA}$  from stellar light and from the AGN continuum emission,  $P_{line}$  and  $P_{line, err}$  represent the measured line parameters for at least three of the narrow lines (narrow H $\beta$ , H $\alpha$ , [O III] doublet, [N II] doublet, [S II] doublet, [O I] doublet). The first criterion ensures the existence of the AGN continuum emission, the second criterion confirms the stellar component, and the third criterion shows there are at least three normal narrow spectral emission lines. Here, the critical values for  $R_{AGN}$  and  $R_{ssp}$  are determined as follows. The value 17% was accepted as the standard flux uncertainty, based on the measured line parameters of the broad balmer lines of the 815 pure type 1 AGNs shown in Figure 3. Therefore, the strength of the AGN continuum emission (stellar lights) is at least twice the uncertainties and indicate there are apparent and reliable AGN continuum emission (stellar lights), thus  $R_{AGN}$  ( $R_{ssp}$ ) should be at least larger than  $\sim 0.30$ .

Using the three criteria above, there are 22693 narrow line objects selected as our spectroscopic sample of the candidates for the BLR-less AGNs. Among the 22693 narrow line objects, 877 objects can be classified as AGNs (Seyfert and LINER objects), 12577 objects can be classified as HII galaxies, based on the BPT line ratios of [O III]/H $\beta$  and [N II]/H $\alpha$ , and 9239 objects can not be classified due to insufficient narrow line information. The BPT diagram can be used to classify the narrow emission line objects. In order to show that the classified HII galaxies by the BPT line ratios can have apparent AGN power law continuum emission, we show the properties of all the 1790 broad line AGNs (including the high luminosity QSOs) having both broad H $\alpha$

and broad  $H\beta$  in the Stripe82 region in the BPT diagram of  $[O\ III]/H\beta$  versus  $[N\ II]/H\alpha$  in Figure 4. Because of the insufficient number of narrow lines, some broad line AGNs in the Stripe82 region are not considered in the BPT diagram. It is clear that even for the broad line AGN, part of the broad line objects lie below the decomposition line between the HII galaxies and AGNs (Seyfert galaxies and LINERs) (Kauffmann et al. 2003, Kewley et al. 2009). Similar results can also be found in Schawinski et al. (2010). Thus, we can reasonably accept the apparent power law continuum component in the spectra of part of the HII galaxies.

Finally, our spectroscopic sample includes 22693 pure narrow line objects (9239 non-classified objects and 13454 classified objects). The objects in the sample have apparent power law continuum emission, apparent narrow spectral emission lines, apparent stellar lights, but no broad lines. The spectral features of the objects are akin to the expected spectral features of the BLR-less AGNs. Besides the spectral features described above, the properties of the photometric variabilities should be used to find the candidates with high confidence levels for the BLR-less AGNs, because variability is one of the fundamental characters of AGN.

### 2.3 Variability-Selection of the BLR-less AGNs

It is convenient to check the properties of the photometry variabilities of the objects in our spectroscopic sample. The photometry light curves spanning over seven years in the Stripe82 database are discussed in detail in Bramich et al. (2008). Through the database provided by Bramich et al. (2008, [http://das.sdss.org/va/stripe\\_82\\_variability/SDSS\\_s2\\_public/](http://das.sdss.org/va/stripe_82_variability/SDSS_s2_public/)), we can conveniently collect the the SDSS five band light curves (with exponential and point spread function (PSF) magnitudes along with uncertainties) and the necessary corresponding parameters on the light curves (such as the rms scatter, object type, Stetson and Vidrih variability indices etc.) for all the objects in the SDSS Stripe82 region. Then, based on the photometry variability properties, the following procedures are applied to find the reliable candidates for the BLR-less AGNs.

It is commonly and well known that there are two important parameters to describe the photometry variabilities and to determine and select the true variable objects: the RMS photometry magnitude deviation ( $RMS$ ) as the function of the magnitude (see the results in Bramich et al. 2008, Kozłowski et al. 2010, and references therein) and the correlation coefficient  $R_{1,2}$  between two different band light curves (see more recent definition in Kozłowski et al. 2010). In this subsection, we check the properties of the two parameters for the pure narrow line objects in our spectroscopic sample, in order to find objects with true and reliable variabilities, which will be our final candidates for the BLR-less AGNs. Certainly, in order to find more reliable RMS magnitude deviations ( $RMS$ ) and correlation coefficients, only the objects having more than 10 reliable photometry observations are considered.

Before proceeding further, some simple descriptions are shown on the parameters of  $RMS$  and  $R_{1,2}$ . Here, the parameter  $R_{1,2}$  is the Pearson's correlation coefficient between two different band light curves, an expected feature of truly variable objects. And, the dependence of the func-

tion of  $RMS$  on photometry magnitude is described as  $RMS = A + B \times \exp(C \times (Mag - 18))$  as posed in Bramich et al. (2008), and then determined as follows. In the plane of photometry magnitude and the RMS, all the spectroscopic objects (galaxies) in the Stripe82 region are binned into 0.1mag. And moreover, in order to ignore the effects of the objects with large variabilities, we only consider the objects having their own standard deviations less than the corresponding RMS magnitude deviation for all objects in the corresponding bin. Then the RMS functions for the SDSS bands are found as

$$\begin{aligned} RMS_g &= 0.039 + 0.004 \times \exp(0.96 \times (Mag_g - 18)) \\ RMS_r &= 0.031 + 0.006 \times \exp(1.01 \times (Mag_r - 18)) \\ RMS_i &= 0.028 + 0.012 \times \exp(0.74 \times (Mag_i - 18)) \end{aligned} \quad (4)$$

Due to the some significantly poorer signal-to-noise for SDSS u and z bands, we mainly consider and show the results on the SDSS gri bands in the manuscript. Figure 5 shows the corresponding results about the  $RMS$  (the solid line the left panels),  $R_{g,r}$  (correlation between g band and r band light curves),  $R_{g,i}$  (correlation between g band and i band light curves) and  $R_{r,i}$  (correlation between r band and i band light curves) for all the galaxies and QSOs in the Stripe82 region.

Then, the determined  $RMS$  function and the calculated  $R_{1,2}$  can be used as the variability indicators, and will mean larger RMS values and higher Pearson's coefficients, for true variabilities:

$$\begin{aligned} RMS_{k,1} &> k_{RMS} \times RMS_{1,M_k} \\ RMS_{k,2} &> k_{RMS} \times RMS_{2,M_k} \\ R_{1,2} &> R_{critical} \end{aligned} \quad (5)$$

, where  $RMS_{k,band}$  and  $RMS_{band,M_k}$  mean the RMS magnitude deviation for the  $k$ th object in the given SDSS band and the calculated RMS photometry magnitude deviation calculated by the  $RMS$  function given the mean photometry magnitude in the given band of the object. Follow the procedures in Kozłowski et al. (2010), we estimate the fraction of the false-positives among the selected objects with true variabilities by

$$f_{fake} = \frac{1 - R_{critical}}{1.5} \times \frac{N_{R_{1,2} < 0.5}}{N_{R_{1,2} > R_{critical}}} \quad (6)$$

where  $N_{R_{1,2} < 0.5}$  ( $N_{R_{1,2} > R_{critical}}$ ) means the number of the selected objects with Pearson's coefficients between two given band light curves smaller than 0.5 (larger than  $R_{critical}$ ). Here, we accept that the weak- or un-correlated objects have the Pearson's coefficient smaller than 0.5. Similar to we adopt, in Kozłowski et al. (2010), the critical value is  $R_{critical} = 0.8$  for highly correlated objects. However, in the manuscript, we require the determined  $f_{fake}$  to be smaller than 10% for our following selected candidates for the BLR-less AGNs, which leads to  $RMS_k > 3 \times RMS_{M_k}$  for three SDSS bands,  $R_{r,i} > R_{critical} \sim 0.75$  for selecting candidates for the BLR-less AGNs through the r and i band results,  $R_{g,r} > R_{critical} \sim 0.85$  for selecting the candidates through the g and r band results and  $R_{g,i} > R_{critical} \sim 0.85$  for selecting the candidates through the g and i band results. Here, the value  $k_{RMS} > 3$  strongly guarantees the variability significance. Then based on the critical values  $R_{critical}$  and the calculated  $RMS$  values, the reliable 281 candidates for the BLR-less AGNs can be selected.

## 2.4 The Final Sample

The 281 reliable candidates for the BLR-less AGNs have the following feature: **true and apparent AGN continuum variabilities, apparent narrow emission lines, and no broad emission lines**. Among the 281 candidates, there are 9 AGNs, 171 HII galaxies and 101 non-classified objects in the SDSS. Meanwhile, the expected number of false-positives among the candidates is less than 30 ( $f_{fake}$  less than 10%). The properties of the RMS functions for the reliable candidates are shown in the left panels in Figure 6. Because only two band light curves out of three three band (SDSS gri bands) light curves are available for some of the candidates. Therefore, in the figure, 133 of the 281 candidates are shown in top left panel, 202 of the 281 candidates are shown in the middle left panel, and 209 of 281 candidates are shown in the bottom left panel. Figure 6 also shows the normal narrow line objects in the spectroscopic sample (contour in solid line in the figure) and all the spectroscopic QSOs with redshift less than 0.35 (contour in dotted line in the figure) in the Stripe82 region. The larger variabilities ( $RMS_k/RMS_{M_k}$ ) of the candidates than those of a large part of QSOs provide further evidence for the true variabilities of the candidates.

Finally, based on both the spectral characters and the photometry variabilities, 281 reliable candidates are included in our final sample. The basic information of the candidates is listed in Table 1, including the SDSS MJD-PLATE-FIBERID information, the redshift, the position, the r band magnitude, the values of  $R_{AGN}$ ,  $R_{1,2}$ ,  $k_{rms}$  and classification.

## 3 DISCUSSIONS AND CONCLUSIONS

Based on the photometry variabilities of the spectroscopic objects from the SDSS Stripe82 region, we selected 281 candidates for the BLR-less AGNs with high confidence levels. We discuss three points/caveats of our spectral analysis below.

First and foremost, the determined power law AGN continuum component is one necessary parameter to select the candidates for the BLR-less AGNs, based on the definition of the BLR-less AGN: the nuclei are directly observed. Thus, the reliability of the AGN continuum determination based on the spectral decomposition, should be carefully further discussed, besides the results shown in the Figure 3. The sum of the pure SSPs gives one power law continuum feature, unless the broadening velocity for the SSPs is unreasonably large or only the much younger SSPs are included. Thus, the parameter  $R_{AGN} > 0.3$  mathematically support the reliability of the power law AGN continuum component. Furthermore, in order to provide clearer evidence for the reliability of the AGN continuum determination, the procedure in the subsection 2.1 is re-applied without the considerations of the AGN continuum component  $P_{AGN,r_\lambda}$  for the observed spectra of the final 281 candidates for the BLR-less AGNs in our final sample. Then, the F-test technique is applied to check the reliability of the AGN component  $P_{AGN,r_\lambda}$ ,

$$F = \frac{(SSE_1 - SSE_2)/(DoF_1 - DoF_2)}{SSE_2/DoF_2} \quad (7)$$

where  $SSE$  represents the sum of squared residuals for one

model, the suffix '1' is for the simple model and '2' is for the slightly complicated model,  $DoF$  represents the degree of freedom for one model. Then, the calculated value  $F$  should be compared to the F-value estimated by the F-distribution with the numerator degrees of freedom of  $DoF_1 - DoF_2$  and the denominator degrees of freedom of  $DoF_2$ . It is clear that the F-value by the F-distribution with  $p = 0.05$  is  $\sim 3$  based on the numerator and denominator degrees of freedom. The calculated  $F$  values through the equation above are much larger than 3, as the shown results in the Figure 7. Thus, the mathematical F-test results support the AGN component  $P_{AGN,r_\lambda}$ .

Second, we simply check the properties of the the intrinsic dust extinction included in the procedure in the subsection 2.1. A detailed discussions of the correlation between the dust extinctions and the other stellar parameters are beyond the scope of the manuscript (more recent detailed discussions can be found in Xiao et al. 2012, Zahid et al. 2013). We discuss one simple result about the dust extinction. Based on the study of starforming galaxies, the mean dust extinction  $E(B-V)$  is around 0.4 and smaller than 1 (due to much weak  $H\beta$ ). In other words, if our procedure from the subsection 2.1 is available for the spectral decomposition, the parameter of the dust extinction should be around 0.4 (see results in Xiao et al. 2012, Zahid et al. 2013 and references therein). Figure 8 shows the distributions of the dust extinctions determined by the procedures with and without the considerations of the component  $P_{AGN,r_\lambda}$ . It is clear that  $E(B-V)$  is around 0.3 with the considerations of  $P_{AGN,r_\lambda}$ , but  $E(B-V)$  is larger than 1 without the considerations of the  $P_{AGN,r_\lambda}$ . Therefore, the AGN component  $P_{AGN,r_\lambda}$  is physically necessary and reliable.

Last but not least, the final point we should make is that there should be no broad emission lines in the SDSS spectra for the 281 candidates for the BLR-less AGNs, based on the definition of BLR-less AGNs. Besides the fitted results as discussed in the subsection 2.1. The final mean spectrum of the candidates for the BLR-less AGNs is discussed. Here, the mean spectrum is determined by the PCA technique (Principal Components Analysis or Karhunen-Loeve Transform method) applied for all the 281 SDSS spectra with the power law continuum and the stellar components having been subtracted. Then the first principal component should represent the mean emission line spectrum of the 281 objects. Figure 9 shows the mean spectrum for the candidates for the 281 BLR-less AGNs. It is clear that there are no broad emission lines. In other words, we can confirm the selected 281 objects have no broad line with the accepted SDSS spectral quality.

Based on the discussions above, we believe although some part of the candidates for the BLR-less AGNs have been lost, due to the spectral quality, the quality of the SDSS Stripe light curves and the strict criteria shown in Equation (5), the selected final candidates for the BLR-less AGNs have high confidence levels. Now, some following basic discussions can be shown for the properties the candidates for the BLR-less AGNs. We firstly check the dependence of the BLR-less AGNs on the luminosity and the accretion rate as discussed in the introduction. Figure 10 shows the distributions of the continuum luminosity at 5100Å for the candidates for the BLR-less AGNs and for the broad line AGNs. The mean values for the continuum luminosi-

ties at 5100Å are  $10^{39.18 \pm 0.76}$  erg/s and  $10^{38.18 \pm 0.85}$  erg/s for the broad line AGNs and the candidates for the BLR-less AGNs respectively. The luminosity ratio between the BLR-less AGNs and normal broad line AGNs is similar as the value shown in Tran (2003), but with larger scatter.

Then, the accretion rate described by the dimensionless Eddington parameter is checked for the normal broad line AGNs and for the candidates for the BLR-less AGNs ( $\dot{M} = L_{bol}/L_{Eddington}$ ), and shown in Figure 10. The mean values of the dimensionless Eddington accretion rate are  $10^{-2.19 \pm 0.98}$  and  $10^{-2.44 \pm 1.02}$  for the broad line AGNs and the candidates for the BLR-less AGNs respectively. Here, the bolometric luminosity is determined by the AGN continuum luminosity (Elvis et al. 1994, Laor 2000, Netzer 2003, Vestergaard 2004, Richards et al. 2006, Marconi et al. 2008), and the Eddington luminosity is determined by the black hole mass through the M-sigma relation (Gebhardt et al., 2000, Ferrarese & Merritt 2001, Tremaine et al. 2002, Gültekin et al. 2009, Woo et al. 2010). The result indicates the accretion rates for the BLR-less AGNs and the normal AGNs are not much different.

Finally, our conclusions are as follows. Based on the SSP templates, the spectra of all the galaxies and QSOs in the SDSS Stripe82 region have been analysed, and then 22693 pure narrow line objects with apparent power law continuum components ( $R_{AGN} > 0.3$  and  $R_{ssp} > 0.3$ ) but no broad emission lines are selected to make up of the spectroscopic sample for the candidates for the BLR-less AGNs. Then, the properties of the photometry variability are checked for the objects in the spectroscopic sample. By the properties of the RMS magnitude deviation ( $RMS$ ) and the Pearson's coefficients ( $R_{1,2}$ ) between two different SDSS band light curves:  $RMS_k > 3 \times RMS_{M_k}$  and  $R_{1,2} > \sim 0.8$ , the final 281 objects are our selected reliable candidates for the BLR-less AGNs, which have reliable photometric variabilities and have reliable AGN continuum emission but do not have broad emission lines. The reported sample four-times enlarges the current sample of the BLR-less AGNs, and will provide more reliable information to explain the lack of the BLRs of AGNs in our following studies.

## ACKNOWLEDGMENTS

Z-XG gratefully acknowledges the anonymous referee for giving us constructive comments and suggestions to greatly improve our paper. Z-XG acknowledges the kind support from the Chinese grant NSFC-11003043 and NSFC-11178003. This paper has made use of the data from the SDSS projects. Funding for the creation and the distribution of the SDSS Archive has been provided by the Alfred P. Sloan Foundation, the Participating Institutions, the National Aeronautics and Space Administration, the National Science Foundation, the U.S. Department of Energy, the Japanese Monbukagakusho, and the Max Planck Society. The SDSS is managed by the Astrophysical Research Consortium (ARC) for the Participating Institutions. The Participating Institutions are The University of Chicago, Fermilab, the Institute for Advanced Study, the Japan Participation Group, The Johns Hopkins University, Los Alamos

National Laboratory, the Max-Planck-Institute for Astronomy (MPIA), the Max-Planck-Institute for Astrophysics (MPA), New Mexico State University, Princeton University, the United States Naval Observatory, and the University of Washington.

## REFERENCES

- Abazajian, K., Adelman-McCarthy, J. K., Agueros, M. A., Allam, S. S., Anderson, S. F., et al., 2009, ApJS, 182, 543  
 Adelman-McCarthy, J. K., Agueros, M. A., Allam, S. S., Anderson, K. S. J., Anderson, S. F., et al., 2008, ApJS, 175, 297  
 Aihara, H., Allende P. C., Deokkeun A., Scott, F. A., Eric, A., et al., 2011, ApJS, 193, 29  
 Antonucci, R., 1993, ARA&A, 31, 473  
 Awaki, H., Ueno, S., Taniguchi, Y., Weaver, K. A., 2000, ApJ, 542, 175  
 Axon, D. J., Hough, J. H., Young, S., Inglis, M., 1994, Ap&SS, 216, 379  
 Bae, H. J., Woo, J. H., Yagi, M., Yoon, S. J., Yoshida, M., 2012, ApJ, 753, 10  
 Baldwin, J. A., Phillips, M. M., & Terlevich, R., 1981, PASP, 93, 5  
 Barth, A. J., Filippenko, A. V., Moran, E. C., 1999a, 515, L61  
 Barth, A. J., Filippenko, A. V., Moran, E. C., 1999b, 525, 673  
 Bauer A., Baltay C., Coppi P., Ellman N., Jerke J., Rabinowitz D., Scalzo R., 2009, ApJ, 696, 1241  
 Bian, W. H., & Gu, Q. S., 2007, ApJ, 657, 159  
 Bianchi, S., Corral, A., Panessa, F., Barcons, X., Matt, G., et al., 2008, MNRAS, 385, 195  
 Bianchi, S., Maiolino, R., Risaliti, G., 2012, Advances in Astronomy, vol. 2012, Article ID 782030  
 Boroson, T., A., & Green, R. F., 1992, ApJS, 80, 109  
 Bramich, D. M., Vidrih, S., Wyrzykowski, L., Munn, J. A., Lin, H., et al., 2008, MNRAS, 386, 887  
 Brightman, M., Nandra, K., 2008, MNRAS, 390, 1241  
 Brinchmann, J., Charlot, S., White, S. D. M., Tremonti, C., Kauffmann, G., Heckman T., 2004, MNRAS, 351, 1151  
 Bruzual, G., & Charlot, S. 2003, MNRAS, 344, 1000  
 Cao, X. W., 2010, ApJ, 724, 855  
 Cappellari, M., McDermid, R. M., Alatalo, K., Blitz, L., Bois, M., et al., 2012, Nature, 484, 485  
 Cid Fernandes, R., Mateus, A., Sodre, L., Stasinska, G., Gomes, J. M., 2005a, MNRAS, 358, 363  
 Cid Fernandes, R., Gu, Q., Melnick, J., Terlevich, E., Terlevich, R., Kunth, D., Rodrigues, L. R., Jouguet, B., 2004, MNRAS, 355, 273  
 Cid Fernandes, R., Gonzalez, D. R. M., Storchi-Bergmann, T., Martins, L. P., Schmitt, H., 2005b, MNRAS, 356, 270  
 Cid Fernandes, R., Asari, N. V., Sodre, L., Stasinska, G., Mateus, A., Torres-Papaqui, J. P., Schoenell, W., 2007, MNRAS, 375, 16  
 Conroy, C., & van Dokkum, P., 2012, ApJ, 747, 69  
 Elitzur, M., & Ho, L. C., 2009, ApJ, 701, L91  
 Elitzur, M., 2012, ApJ, 747, L33  
 Elvis M., Belinda J., McDowell J. C., et al. 1994, ApJS, 95, 1  
 Fan X. H., 1999, AJ, 117, 2528

- Fan X. H., Strauss M. A., Becker R. H., et al., 2006, *AJ*, 132, 117
- Ferrarese L. & Merritt D., 2001, *MNRAS*, 320, L30
- Gebhardt K., Bender R., Bower G., Dressler A., Faber S. M., et al., 2000, *ApJ*, 439, L13
- Georgantopoulos, I., & Zezas, A., 2003, *ApJ*, 594, 704
- Ghosh, H., Pogge, R. W., Mathur, S., Martini, P., Shields, J. C., 2007, *ApJ*, 656, 105
- Giraud, E., Melnick, J., Gu, Q. S., Quintana, H., Selman, F., Toledo, I., Zelaya, P., 2011, *Advances in Astronomy*, 2011, 5
- Gliozzi, M., Sambruna, R. M., Foschini, L., 2007, *ApJ*, 662, 878
- Gliozzi, M., Panessa, F., La Franca, F., Saviane, I., Monaco, L., et al., 2010, *ApJ*, 725, 2071
- Greene, J. E., & Ho, L. C., 2005, *ApJ*, 627, 721
- Gültekin K., Richstone D. O., Gebhardt K., Lauer T. R., Tremaine S., et al., 2009, *ApJ*, 698, 198
- Hao, L., Strauss, M. A., Tremonti, C. A., Schlegel, D. J., Heckman, T. M., et al., 2005, *AJ*, 129, 1783
- Hawkins, M. R. S., 2004, *A&A*, 424, 519
- Hawkins, M. R. S., 2007, *A&A*, 462, 581
- Heisler, C. A., Lumsden, S. L., Bailey, J. A., 1997, *Nature*, 385, 700
- Hiner, K. D., Canalizo, G., Lacy, M., Sajina, A., Armus, L., et al., 2009, *ApJ*, 706, 508
- Ivezic, Z., Smith, J. A., Miknaitis, G., Lin, H., Tucker, D., et al., 2007, *AJ*, 134, 973
- Kay, L. E., 1994, *ApJ*, 430, 196
- Kay, L. E., & Moran, E. C., 1998, *PASP*, 110, 1003
- Kauffmann, G., Heckman, T. M., Tremonti, C., et al. 2003, *MNRAS*, 346, 1055
- Kelly B. C., Bechtold J., Siemiginowska A. 2009, *ApJ*, 698, 895
- Kewley, L. J., Dopita, M. A., Sutherland, R. S., Heisler, C. A., Trevena, J., 2001, *ApJ*, 556, 121
- Kewley, L. J., Groves, B., Kauffmann, G., Heckman, T., 2006, *MNRAS*, 372, 961
- Kovacevic, J., Popovic, L. C., Dimitrijevic, M. S., 2010, *ApJS*, 189, 15
- Kozłowski S., Kochanek C. S., Udalski A., Wyrzykowski L., Soszynski I., et al., 2010, *ApJ*, 708, 927
- Laor A. 2000, *ApJ*, 543, L111
- Laor, A., 2003, *ApJ*, 590, 86
- Li, C., Wang, T. G., Zhou, H. Y., Dong, X. B., Chen, F. Z., 2005, *AJ*, 129, 669
- Lutz, D., Genzel, R., Sturm, E., Tacconi, L., Wiprecht, E., Alexander, T., et al., 2000, *ApJ*, 530, 733
- Malizia, A., Bassani, L., Bazzano, A., Bird, A. J., Masetti, N., Panessa, F., Stephen, J. B., Ubertini, P., 2012, 426, 1750
- Maraston, C., & StrOmbAck, G., 2011, *MNRAS*, 418, 2785
- Marconi A., Axon D. J., Maiolino R., et al. 2008, *ApJ*, 678, 693
- Marinucci, A., Bianchi, S., Nicastro, F., Matt, G., Goulding, A. D., 2012, *ApJ*, 748, 130
- Miller, J. S., & Goodrich, R. W., 1990, *ApJ*, 355, 456
- Moran, E. C., Barth, A. J., Kay, L. E., Filippenko, A. V., 2000, *ApJ*, 540, L73
- Nagao, T., Kawabata, K. S., Murayama, T., Ohyama, Y., Taniguchi, Y., et al., 2004, *AJ*, 128, 109
- Netzer H. 2003, *ApJ*, 583, L5
- Nicastro, F., 2000, *ApJ*, 530, L65
- Nicastro, F., Martocchia, A., Matt, G., 2003, *ApJ*, 589, L13
- Panessa, F., & Bassani, L., 2002, *A&A*, 394, 435
- Panessa, F., Carrera, F. J., Bianchi, S., Corral, A., Gastaldello, F., et al., 2009, *MNRAS*, 398, 1951
- Peacock M. B., Zepf S. E., Maccarone T. J., KUndu A., 2011, *ApJ*, 737, 5
- Petrov, G. P., & Yankulova, I. M., 2012, *New Astronomy*, 17, 137
- Plotkin, R. M., Anderson, S. F., Brandt, W. N., Diamond-Stanic, A. M., Fan, X., et al., 2010, *ApJ*, 721, 562
- Rees, M. J., 1984, *ARA&A*, 22, 471
- Richards J. W., Freeman P. E., Lee A. B., Schafer C. M., 2009, *MNRAS*, 399, 1044
- Schawinski K., Urry C. M., Virani S., et al., 2010, *ApJ*, 711, 284
- Schmidt, G. D., Smith, P. S., Foltz, C. B., Hines, D. C., 2002, *ApJ*, 578, L99
- Seymour, N., Stern, D., De Breuck, C., Vernet, J., Rettura, A., et al., 2007, *ApJS*, 171, 353
- Shemmer, O., Brandt, W. N., Schneider, D. P., Fan, X., Strauss, M. A., et al., 2006, *ApJ*, 644, 86
- Shi, Y., Rieke, G. H., Smith, P., Rigby, J., Hines, D., et al., 2010, *ApJ*, 714, 115
- Sigut, T. A. A., & Pradhan, A. K., 2003, *ApJS*, 145, 15
- Smolcic, V., & Riechers, D. A., 2011, *ApJ*, 730, 64
- Stasinska, G., Cid Fernandes, R., Mateus, A., Sodre, L., Asari, N. V., 2006, *MNRAS*, 371, 972
- Tran, H. D., 2001, *ApJ*, 554, L19
- Tran, H. D., 2003, *ApJ*, 583, 632
- Tran, H. D., Lyke, J. E., Mader, J. A., 2011, *ApJ*, 726, L21
- Tremaine S., Gebhardt K., Bender R., Bower, G., Dressler A., et al., 2002, *ApJ*, 574, 740
- Tremonti, C. A., Heckman, T. M., Kauffmann, G., Brinchmann, J., Charlot, S., et al., 2004, *ApJ*, 613, 898
- Urry, M. C., & Padovani, P., 1995, *PASP*, 107, 803
- Vanden Berk, D. E., Shen, J. J., Yip, H. W., Schneider, D. P., et al., 2006, *AJ*, 131, 84
- Vazdekis, A., Sanchez-Blazquez, P., Falcon-Barroso, J., Cenarro, A. J., Beasley, M. A., Cardiel, N., Gorgas, J., Peletier, R. F., 2010, *MNRAS*, 404, 1639
- Veilleux, S., & Osterbrock D. E., 1987, *ApJS*, 63, 295
- Veilleux, S., Sanders, D. B., Kim, D. C., 1997, *ApJ*, 484, 92
- Veilleux, S., Sanders, D. B., Kim, D. C., 1999, *ApJ*, 522, 139
- Vestergaard M. 2004, *ApJ*, 601, 676
- Vidrih, S., Bramich, D. M., Hewett, P. C., Evans, N. W., Gilmore, G., et al., 2007, *MNRAS*, 382, 515
- Wang, J. M., & Zhang, E. P., 2007, *ApJ*, 660, 1072
- Wilkins S. M., Gonzalez-Perez V., Lacey C. G., Baugh C. M., 2012, *MNRAS*, 424, 1522
- Wolter, A., Gioia, I. M., Henry, J. P., Mullis, C. R., 2005, *A&A*, 444, 165
- Woo J. H. Treu T., Barth A. J., Wright S. A., Walsh J. L., et al., 2010, *ApJ*, 716, 269
- Wu, Y. Z., Zhang, E. P., Liang, Y. C., Zhang, C. M., Zhao, Y. H., 2011, *ApJ*, 730, 121
- Xiao T., Wang T. G., Wang H. Y., Zhou H. Y., Lu H. L., Dong X. B., 2012, *MNRAS*, 421, 486
- Yip, C. W., Connolly, A. J., Vanden Berk, D. E., Ma, Z., Frieman, J. A., et al., 2004, *AJ*, 128, 2603

- York, D. G., Adelman J., Anderson, J. E., Anderson, S. F.,  
Annis, J., et al., 2000, *AJ*, 120, 1579
- Young, S., Hough, J. H., Efstathiou, A., Wills, B. J., Axon,  
D. J., Bailey, J. A., Ward, M. J., 1996, *MNRAS*, 279, L72
- Young, S., Axon, D. J., Hough, J. H., Fabian, A. C., Ward,  
M. J., 1998, *MNRAS*, 294, 478
- Yu, P. C., & Hwang, C. Y., 2011, *AJ*, 142, 14
- Zahid H. J., Yates R. M., Kewley L. J., Kudritzki R. P.,  
2013, *ApJ*, 763, 92
- Zhang, E. P., & Wang, J. M., 2006, *ApJ*, 653, 137
- Zhang, X. G., Dultzin D., Wang, T. G., 2008, *MNRAS*,  
385, 1087

**Table 1.** Basic Parameters of the 281 candidates for the BLR-less AGNs

mpf	z	ra	dec	mag	$R$	$k$	$R_{1,2}$	cl	mpf	z	ra	dec	mag	$R$	$k$	$R_{1,2}$	cl
51782-0391-236	0.080	6.91631	-0.61917	17.1	0.38	9.41	0.99	hii	51782-0391-460	0.069	6.88574	0.723382	17.3	0.31	8.30	0.98	non
51782-0391-625	0.013	8.31179	0.201018	15.6	0.47	23.7	0.99	hii	51783-0385-214	0.019	355.184	-0.88746	17.8	0.58	10.4	0.98	hii
51783-0395-413	0.007	14.4857	0.869196	17.1	0.40	22.0	0.97	non	51788-0373-490	0.116	331.793	0.537971	17.7	0.42	6.33	0.76	non
51788-0401-400	0.052	24.7862	0.349467	17.3	0.48	20.6	0.99	non	51788-0401-547	0.084	26.0518	0.517921	17.6	0.38	3.28	0.89	non
51789-0379-160	0.127	343.729	0.065114	18.9	0.35	7.73	0.97	non	51789-0379-537	0.025	343.643	0.830080	16.1	0.38	11.7	0.97	hii
51789-0398-127	0.073	19.6826	-0.88279	20.3	0.48	23.4	0.93	hii	51789-0398-180	0.047	19.7441	-0.43511	16.9	0.32	6.09	0.96	hii
51789-0398-501	0.089	19.3185	0.502616	17.5	0.36	20.5	0.98	non	51791-0374-419	0.090	333.474	0.880517	17.3	0.54	3.79	0.92	non
51793-0388-119	0.074	2.54452	-0.31131	17.6	0.48	6.92	0.94	non	51793-0388-614	0.108	2.78680	0.845443	17.1	0.53	4.79	0.89	hii
51793-0392-262	0.116	8.55825	0.039864	17.5	0.34	6.67	0.99	non	51793-0392-284	0.006	8.34204	-1.12137	16.3	0.42	59.0	0.90	hii
51794-0397-008	0.018	18.8170	-1.10024	16.8	0.42	6.97	0.94	non	51794-0397-336	0.003	17.2832	1.120985	16.4	0.62	7.76	0.97	hii
51795-0389-064	0.069	4.61792	-0.56956	16.6	0.42	6.05	0.94	hii	51811-0381-353	0.054	346.277	0.410307	17.9	0.37	5.08	0.89	hii
51812-0394-372	0.042	12.2676	0.765777	17.6	0.30	16.4	0.97	non	51812-0394-442	0.066	12.9475	0.989699	16.3	0.39	10.4	0.83	non
51812-0404-462	0.076	31.0442	0.526773	18.4	0.44	5.36	0.94	hii	51816-0382-010	0.024	350.466	-0.69467	18.2	0.48	24.5	0.97	hii
51816-0382-083	0.091	349.658	-1.22573	17.2	0.33	7.33	0.95	hii	51816-0382-185	0.024	348.901	-0.45154	16.8	0.38	4.47	0.97	non
51816-0382-564	0.030	349.966	1.218043	16.3	0.47	4.25	0.95	non	51816-0390-348	0.017	4.47590	0.329340	17.0	0.31	16.3	0.99	hii
51816-0390-409	0.016	5.10742	0.826350	14.0	0.35	15.7	0.99	agn	51816-0396-011	0.076	16.9530	-1.01500	18.3	0.33	12.2	0.98	hii
51816-0396-204	0.019	16.1731	-0.95594	15.0	0.39	22.3	0.99	hii	51816-0396-271	0.067	15.4541	-0.15510	17.8	0.41	4.20	0.97	hii
51817-0399-196	0.043	20.7603	-0.32410	15.8	0.35	5.25	0.98	non	51817-0399-323	0.008	20.5265	0.938026	19.8	0.38	26.3	0.96	hii
51817-0399-324	0.007	20.5577	0.958729	17.3	0.51	48.7	0.96	hii	51817-0399-434	0.121	20.7876	0.166059	18.2	0.65	16.0	0.97	agn
51817-0399-469	0.067	20.8725	0.568883	16.5	0.33	4.31	0.97	hii	51817-0406-066	0.021	36.5963	-0.49192	17.4	0.44	12.8	0.95	non
51817-0411-119	0.029	46.5573	-0.34154	16.4	0.37	19.7	0.99	non	51818-0383-222	0.115	350.824	-0.23943	16.8	0.51	9.02	0.98	non
51820-0407-023	0.245	39.1133	-0.61284	18.8	0.33	10.9	0.94	non	51820-0407-320	0.021	36.5963	-0.49192	17.4	0.35	12.8	0.95	hii
51820-0407-509	0.021	38.1587	0.594263	15.6	0.63	5.02	0.97	hii	51821-0384-257	0.083	352.805	-0.93731	17.7	0.50	28.7	0.90	hii
51821-0384-278	0.008	352.758	-0.13197	17.2	0.40	23.4	0.99	non	51869-0406-063	0.021	36.5963	-0.49192	17.4	0.36	12.8	0.95	hii
51871-0403-237	0.027	29.0007	-0.36291	17.0	0.32	20.5	0.98	hii	51871-0403-452	0.081	29.5011	1.089686	17.1	0.32	4.16	0.96	hii
51871-0403-621	0.111	31.0741	0.710236	17.2	0.34	8.88	0.92	hii	51871-0409-114	0.021	42.4203	-0.52336	14.5	0.32	9.19	0.95	hii
51871-0409-237	0.005	41.6048	-0.49868	12.2	0.46	45.2	0.99	hii	51871-0409-298	0.043	41.2430	-0.94640	16.7	0.31	23.0	0.90	hii
51871-0409-465	0.075	41.9021	0.451147	17.8	0.48	3.52	0.89	non	51871-0412-075	0.025	48.4493	-0.24329	18.2	0.67	40.9	0.99	non
51871-0412-581	0.025	48.3041	0.282182	17.5	0.34	11.4	0.92	hii	51873-0411-101	0.029	46.5573	-0.34154	16.4	0.36	19.7	0.99	hii
51876-0394-489	0.115	13.0620	0.583035	16.9	0.40	20.7	0.94	agn	51876-0394-508	0.147	13.5640	0.271241	18.3	0.31	4.70	0.92	non
51876-0394-565	0.041	13.5639	1.077725	16.1	0.36	18.8	0.99	non	51876-0406-063	0.021	36.5963	-0.49192	17.4	0.43	12.8	0.95	non
51877-0385-211	0.019	355.184	-0.88746	17.8	0.42	10.4	0.98	hii	51877-0404-470	0.076	31.0442	0.526773	18.4	0.60	5.36	0.94	hii
51900-0390-350	0.017	4.47590	0.329340	17.0	0.34	16.3	0.99	hii	51900-0390-407	0.016	5.10742	0.826350	14.0	0.32	15.7	0.99	agn
51900-0406-063	0.021	36.5963	-0.49192	17.4	0.47	12.8	0.95	hii	51913-0394-569	0.041	13.5639	1.077725	16.1	0.40	18.8	0.99	hii
51929-0413-196	0.066	49.4594	-0.12439	16.1	0.32	3.05	0.94	hii	51929-0413-356	0.025	48.3041	0.282182	17.5	0.45	11.4	0.92	hii
51931-0412-009	0.027	48.6088	-1.14626	17.3	0.33	7.95	0.97	non	51931-0412-588	0.025	48.3041	0.282182	17.5	0.39	11.4	0.92	hii
51936-0412-009	0.027	48.6088	-1.14626	17.3	0.52	7.95	0.97	non	51936-0412-582	0.025	48.3041	0.282182	17.5	0.44	11.4	0.92	hii
51942-0412-016	0.027	48.6088	-1.14626	17.3	0.33	7.95	0.97	hii	51942-0412-582	0.025	48.3041	0.282182	17.5	0.56	11.4	0.92	hii
52078-0371-243	0.122	327.225	-1.16658	18.9	0.31	4.27	0.89	hii	52143-0376-576	0.055	338.028	0.915153	17.8	0.53	6.63	0.96	non
52145-0377-372	0.059	338.816	0.892289	17.2	0.31	3.45	0.84	hii	52146-0378-104	0.015	341.767	-0.07408	14.5	0.34	31.7	0.98	non
52146-0378-277	0.058	340.269	-0.07247	17.8	0.34	22.6	0.99	hii	52146-0378-347	0.005	340.391	0.400612	15.1	0.38	55.2	0.99	non
52174-0676-265	0.212	342.081	-0.61156	17.9	0.31	5.24	0.95	non	52174-0676-408	0.048	343.019	1.246003	18.1	0.40	19.5	0.93	hii
52175-0708-264	0.021	42.4203	-0.52336	14.5	0.30	9.19	0.95	hii	52175-0708-419	0.059	43.2783	1.161945	17.3	0.36	11.1	0.96	hii
52177-0679-157	0.233	348.889	-0.10358	19.9	0.38	3.77	0.93	hii	52177-0707-507	0.075	41.9021	0.451147	17.8	0.48	3.52	0.89	hii
52178-0676-360	0.085	341.789	0.175907	17.0	0.32	5.74	0.98	non	52178-0676-410	0.048	343.019	1.246003	18.1	0.60	19.5	0.93	hii
52178-0676-532	0.025	343.643	0.830053	16.1	0.38	11.7	0.97	hii	52178-0676-552	0.127	343.729	0.065114	18.9	0.40	7.73	0.97	hii
52199-0681-139	0.023	352.971	-0.82643	16.9	0.39	56.8	0.99	hii	52199-0691-527	0.064	11.7256	1.011370	17.4	0.32	8.03	0.99	non
52200-0680-166	0.115	350.824	-0.23943	16.8	0.35	9.02	0.98	agn	52200-0705-486	0.326	37.6558	0.189943	19.9	0.30	6.25	0.92	non
52201-0674-347	0.059	337.764	0.283131	17.7	0.33	24.8	0.99	hii	52201-0692-278	0.309	12.6371	-0.39110	19.4	0.46	5.34	0.93	hii
52202-0695-105	0.047	19.6483	-0.23312	15.1	0.33	22.8	0.99	hii	52202-0695-325	0.003	18.2318	0.991891	18.0	0.66	27.5	0.97	hii
52202-0695-413	0.064	18.5338	0.846754	17.7	0.37	4.68	0.86	hii	52202-0699-432	0.084	26.0518	0.517921	17.6	0.33	3.28	0.89	hii
52202-0711-485	0.022	49.3344	-0.07717	16.6	0.34	60.2	0.99	hii	52203-0688-304	0.069	4.61792	-0.56956	16.6	0.36	6.05	0.94	agn
52203-0688-391	0.105	5.12084	0.300712	18.6	0.35	3.09	0.91	hii	52205-0704-383	0.291	34.9974	0.159337	19.1	0.45	8.56	0.78	non
52205-0704-482	0.327	35.9311	0.552009	19.5	0.50	13.3	0.99	hii	52205-0709-065	0.119	46.5204	-0.46675	18.1	0.34	9.79	0.97	non
52209-0696-406	0.055	20.5731	1.007560	16.1	0.44	11.1	0.96	hii	52209-0696-515	0.056	21.1558	0.087213	17.9	0.32	21.9	0.88	hii
52226-0697-508	0.080	22.8879	0.552905	19.6	0.39	24.6	0.94	non	52235-0412-079	0.025	48.4493	-0.24329	18.2	0.62	40.9	0.99	non
52235-0412-587	0.025	48.3041	0.282182	17.5	0.36	11.4	0.92	hii	52250-0412-586	0.025	48.3041	0.282182	17.5	0.33	11.4	0.92	hii
52254-0412-004	0.027	48.6088	-1.14626	17.3	0.44	7.95	0.97	hii	52254-0412-072	0.025	48.4493	-0.24329	18.2	0.56	40.9	0.99	hii

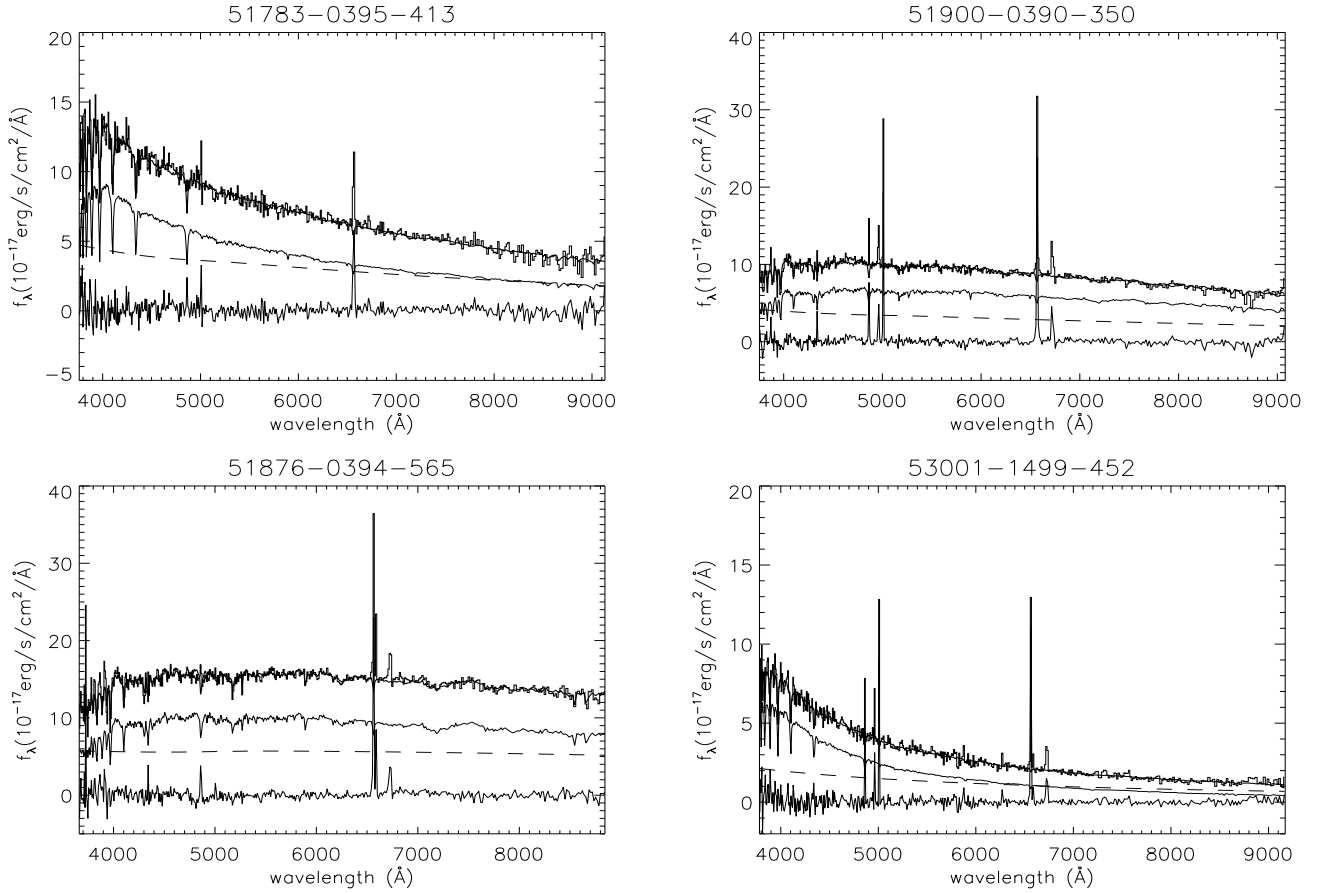
Notice: The first and the tenth columns list the SDSS MJD-PLATE-FIBERID, the second and eleventh columns show the redshift, the third and twelfth columns show the ra value in degree, the fifth and thirteenth columns show the dec values in degree, the sixth and fourteenth columns show the magnitudes in r band, the seventh and fifteenth columns show the parameter  $R_{AGN}$ , the eighth and sixteenth columns show the maximum values of  $k_{RMS} = RMS_k/RMS_{M_k}$  in the SDSS gri bands, the ninth and seventeenth columns show maximum values of Spearman's correlation coefficient  $R_{1,2}$ , and the tenth and final columns show the classifications for the objects: AGNs (agn), HII galaxies (hii) or non-classified objects (non).

Table 1. –continued.

mpf	z	ra	dec	mag	$R$	$k$	$R_{1,2}$	cl	mpf	z	ra	dec	mag	$R$	$k$	$R_{1,2}$	cl
52254-0412-591	0.025	48.3041	0.282182	17.5	0.36	11.4	0.92	hii	52254-0693-367	0.018	14.7013	0.589705	18.5	0.45	57.4	0.99	non
52258-0412-079	0.025	48.4493	-0.24329	18.2	0.68	40.9	0.99	hii	52258-0412-587	0.025	48.3041	0.282182	17.5	0.37	11.4	0.92	hii
52261-0690-587	0.218	10.7037	0.578405	18.8	0.43	4.78	0.94	hii	52261-0690-609	0.018	10.4392	1.174548	17.9	0.45	37.3	0.98	non
52262-0689-064	0.067	8.37281	-0.54093	18.0	0.48	11.0	0.97	non	52262-0689-070	0.106	8.37799	-0.32262	18.8	0.54	4.35	0.92	hii
52264-0803-154	0.138	47.8015	-0.28485	18.5	0.36	10.3	0.96	hii	52264-0803-320	0.119	46.5204	-0.46675	18.1	0.40	9.79	0.97	non
52286-0804-294	0.141	48.7204	-0.64079	18.6	0.31	9.03	0.92	non	52286-0804-429	0.151	49.0715	0.465250	18.9	0.47	7.36	0.89	non
52289-0802-348	0.043	44.8906	0.915088	18.6	0.51	10.8	0.89	non	52289-0802-453	0.199	45.3461	0.476043	18.9	0.47	6.06	0.89	hii
52297-0803-561	0.209	48.3019	0.532733	18.1	0.38	3.92	0.91	non	52297-0803-600	0.156	48.2579	0.725732	20.9	0.44	4.11	0.85	non
52318-0803-136	0.138	47.8015	-0.28485	18.5	0.30	10.3	0.96	hii	52318-0803-290	0.119	46.5204	-0.46675	18.1	0.39	9.79	0.97	hii
52318-0803-334	0.138	46.3641	0.128511	19.3	0.51	4.96	0.84	non	52435-0981-046	0.080	310.852	-0.17299	17.1	0.34	12.6	0.98	hii
52443-0983-360	0.130	312.062	0.145880	17.8	0.44	6.60	0.95	non	52465-0990-307	0.063	324.507	-0.40264	17.4	0.32	14.3	0.99	non
52465-0990-443	0.068	325.760	1.242723	17.1	0.39	3.16	0.86	non	52466-0982-127	0.118	312.025	-0.23095	17.8	0.37	13.5	0.99	non
52468-0989-230	0.120	323.220	-0.39948	17.4	0.34	13.5	0.99	hii	52518-0687-534	0.303	4.27962	0.966183	19.4	0.55	5.32	0.91	hii
52520-0670-308	0.300	15.2634	-0.36469	19.8	0.38	5.03	0.84	non	52520-0988-498	0.063	322.660	0.254061	17.4	0.44	9.73	0.89	hii
52520-0988-560	0.049	322.772	0.953709	17.8	0.33	5.40	0.96	hii	52521-1095-198	0.008	351.088	-0.10817	18.6	0.63	7.88	0.94	hii
52521-1095-349	0.031	349.876	0.371450	19.2	0.58	38.4	0.98	hii	52523-0684-042	0.111	358.723	-1.08919	19.2	0.40	5.10	0.94	hii
52523-1082-567	0.047	16.8977	1.194968	18.0	0.42	3.42	0.94	hii	52524-1022-156	0.120	312.239	-0.43634	18.5	0.48	11.9	0.90	hii
52524-1022-227	0.216	311.452	-0.60317	18.3	0.30	6.01	0.90	non	52524-1022-415	0.027	311.455	0.674695	17.7	0.46	6.12	0.80	hii
52525-1034-601	0.112	334.940	0.375554	18.9	0.42	5.28	0.95	non	52525-1034-625	0.057	334.453	1.070917	19.5	0.37	5.96	0.96	non
52527-0669-307	0.283	0.66073	-0.20296	19.6	0.33	5.58	0.87	hii	52531-1081-048	0.005	18.8768	-0.86274	16.5	0.49	70.6	0.93	non
52531-1085-368	0.017	10.4457	1.172180	18.7	0.53	40.0	0.98	hii	52557-1027-034	0.293	321.683	-0.66242	19.5	0.61	3.55	0.82	non
52557-1027-111	0.124	320.953	-0.91073	18.5	0.32	11.6	0.96	non	52557-1027-200	0.124	320.899	-0.89219	19.0	0.49	5.06	0.89	hii
52557-1027-309	0.010	319.555	-0.86333	18.3	0.33	6.14	0.90	non	52557-1027-452	0.086	320.542	0.392080	18.5	0.52	19.3	0.98	non
52558-1026-178	0.340	318.844	-0.20190	19.0	0.31	5.91	0.93	non	52558-1026-280	0.060	317.996	-0.22021	17.2	0.39	7.69	1.00	agn
52559-0669-301	0.283	0.66073	-0.20296	19.6	0.61	5.58	0.87	non	52562-1028-489	0.030	322.438	0.678383	19.4	0.59	12.3	0.98	hii
52582-1036-211	0.059	337.244	-1.00362	18.4	0.38	10.7	0.98	hii	52582-1036-271	0.055	336.923	-0.15137	18.1	0.39	3.87	0.93	hii
52582-1036-528	0.037	337.988	1.095786	17.7	0.45	18.7	0.98	hii	52589-1066-160	0.138	47.8020	-0.28447	20.9	0.33	3.75	0.75	non
52590-0675-225	0.127	340.831	-0.35270	18.0	0.36	5.34	0.96	hii	52590-0675-331	0.089	340.445	1.201112	17.5	0.41	4.54	0.99	hii
52590-0675-540	0.016	341.517	0.937274	17.5	0.52	11.3	0.98	non	52590-1069-193	0.005	41.6056	-0.49924	17.2	0.48	30.9	0.96	hii
52590-1069-621	0.028	42.9714	0.665730	20.7	0.49	10.0	0.92	hii	52591-1070-536	0.023	40.2009	1.101998	19.9	0.69	16.4	0.85	hii
52591-1084-099	0.062	12.8838	-0.76888	19.0	0.62	10.4	0.82	hii	52591-1084-407	0.015	12.4672	0.963360	14.6	0.34	3.47	0.96	hii
52616-1067-066	0.024	46.3729	-0.38143	16.8	0.43	70.4	0.85	hii	52637-1179-039	0.027	48.6088	-1.14626	17.3	0.34	7.95	0.97	hii
52637-1179-048	0.025	48.4493	-0.24329	18.2	0.49	40.9	0.99	hii	52639-1092-600	0.081	358.352	0.060815	18.4	0.41	14.0	0.99	hii
52641-1071-457	0.021	37.6254	0.379881	18.1	0.39	10.9	0.96	hii	52643-1078-118	0.015	23.8070	-1.17728	18.6	0.41	5.33	0.87	hii
52643-1078-458	0.016	23.2780	0.177129	19.7	0.68	20.3	0.90	hii	52669-0811-252	0.037	47.1443	-0.85147	19.3	0.48	7.45	0.91	non
52669-0811-415	0.030	47.2661	0.646299	19.3	0.48	6.69	0.92	hii	52669-0811-490	0.048	47.8897	0.533254	18.4	0.53	9.67	0.98	hii
52669-0811-634	0.151	49.0715	0.465250	18.9	0.46	7.36	0.89	non	52797-1023-295	0.129	312.590	-1.00562	18.6	0.37	7.31	0.97	non
52797-1023-389	0.200	312.525	0.558429	18.8	0.36	15.7	0.75	agn	52797-1023-510	0.201	313.706	0.697158	19.5	0.34	4.68	0.81	non
52813-1034-254	0.131	333.099	-0.96498	18.1	0.32	6.24	0.99	non	52813-1034-604	0.057	334.453	1.070917	19.5	0.31	5.96	0.96	non
52816-1035-031	0.090	336.789	-0.62212	18.1	0.40	16.6	0.99	hii	52816-1035-572	0.057	336.033	0.861933	18.2	0.37	13.0	0.99	hii
52822-1033-140	0.095	331.749	-0.88593	18.9	0.31	8.36	0.99	hii	52822-1033-198	0.207	331.462	-0.11459	19.6	0.58	4.68	0.90	hii
52826-1024-216	0.133	314.818	-0.78427	19.1	0.39	6.30	0.90	non	52826-1024-365	0.027	314.454	1.079220	18.9	0.47	7.98	0.92	hii
52826-1024-536	0.056	315.207	1.190049	17.8	0.37	11.3	0.92	non	52826-1037-503	0.160	339.814	0.317021	19.6	0.48	6.48	0.94	hii
52826-1037-587	0.058	340.770	0.356819	18.1	0.31	31.6	0.75	non	52878-1037-376	0.060	338.955	0.537190	19.1	0.31	22.1	0.75	non
52878-1037-604	0.059	340.390	0.817578	18.8	0.43	4.78	0.84	hii	52883-1496-181	0.059	12.4817	-0.20429	18.9	0.31	9.20	0.98	hii
52884-1028-111	0.129	322.510	-0.99479	18.9	0.47	14.2	0.98	non	52884-1028-391	0.031	321.707	0.975860	18.4	0.47	8.30	0.94	non
52884-1028-471	0.030	322.438	0.678383	19.4	0.47	12.3	0.98	hii	52886-1497-450	0.017	14.7330	1.005642	18.5	0.51	29.2	0.97	hii
52886-1497-529	0.017	14.9293	0.921629	19.2	0.50	17.8	0.94	hii	52903-1090-042	0.031	2.52555	-0.43833	17.8	0.51	27.8	0.96	non
52903-1090-346	0.076	0.81866	1.085157	18.3	0.44	6.65	0.79	hii	52903-1475-374	0.009	331.180	1.039517	18.3	0.59	8.56	0.88	non
52903-1475-555	0.154	332.219	0.285299	20.9	0.34	4.95	0.85	agn	52912-1029-094	0.118	324.504	-0.62392	18.8	0.34	5.23	0.94	hii
52912-1029-194	0.026	323.662	-0.16645	18.3	0.48	6.97	0.93	hii	52912-1029-550	0.166	324.588	0.284699	19.6	0.39	3.46	0.86	hii
52912-1106-456	0.010	329.737	1.018632	18.7	0.55	19.3	0.89	hii	52914-1030-159	0.075	326.072	-0.24196	19.4	0.32	7.15	0.88	hii
52914-1498-075	0.226	17.1398	-0.46871	18.8	0.49	8.59	0.94	hii	52930-1087-005	0.067	7.65952	-0.92077	19.1	0.56	28.7	0.99	hii
52930-1087-112	0.040	7.41983	-0.41391	18.3	0.49	7.26	0.91	non	52930-1087-123	0.066	6.87844	-1.19850	18.2	0.45	5.85	0.76	hii
52930-1087-157	0.068	7.32642	-0.08815	19.7	0.48	26.3	0.99	hii	52930-1087-543	0.059	7.43631	0.776922	17.9	0.31	12.0	0.99	hii
52931-1514-187	0.227	47.4285	-0.26699	19.3	0.31	4.91	0.93	hii	52931-1514-219	0.037	47.4941	-0.69401	21.2	0.47	8.77	0.87	hii
52931-1514-625	0.131	49.2046	0.084835	21.0	0.67	7.22	0.91	non	52932-1515-301	0.025	48.4502	-0.24319	18.9	0.59	47.1	0.99	non
52932-1515-359	0.025	48.3037	0.282169	17.5	0.32	11.4	0.92	hii	52932-1522-500	0.183	320.470	0.468425	18.2	0.37	10.3	0.95	non
52933-1075-095	0.052	29.8693	-0.96168	18.3	0.35	8.11	0.98	non	52933-1075-464	0.022	29.6694	0.522198	19.6	0.53	22.1	0.98	hii
52933-1075-546	0.040	30.3278	0.451110	17.8	0.40	5.75	0.95	hii	52933-1474-189	0.016	329.601	-0.73713	20.4	0.57	10.8	0.86	hii
52933-1493-628	0.072	8.19787	0.544704	18.7	0.40	7.40	0.94	hii	52937-1494-342	0.094	7.84317	0.309932	19.3	0.52	8.33	0.96	non
52937-1494-563	0.068	9.50234	1.120122	18.3	0.30	6.45	0.96										

**Table 1.** –continued.

mpf	z	ra	dec	mag	<i>R</i>	<i>k</i>	<i>R</i> <sub>1,2</sub>	cl	mpf	z	ra	dec	mag	<i>R</i>	<i>k</i>	<i>R</i> <sub>1,2</sub>	cl
52946-1511-290	0.054	41.2201	-0.85115	18.8	0.40	5.15	0.94	non	52964-1476-602	0.057	334.453	1.070917	19.5	0.34	5.96	0.96	non
52964-1487-229	0.068	355.029	-0.48348	18.8	0.39	9.85	0.95	hii	52965-1488-347	0.023	356.157	0.177964	19.0	0.44	4.61	0.86	hii
52974-1096-212	0.068	348.910	-0.68242	18.8	0.31	8.58	0.86	non	52974-1096-283	0.012	348.466	-1.17533	18.5	0.36	7.61	0.86	hii
52991-1489-096	0.026	359.951	-0.76895	19.0	0.52	8.37	0.77	hii	52991-1564-218	0.155	47.6880	-0.64722	19.1	0.32	4.57	0.95	hii
52993-1486-448	0.027	353.154	1.223620	18.8	0.53	5.72	0.87	non	52994-1490-111	0.074	2.54401	-0.31029	18.8	0.44	5.44	0.98	hii
52996-1491-501	0.040	3.57930	0.200984	19.2	0.50	14.9	0.95	hii	53001-1499-014	0.005	18.8829	-0.86236	16.5	0.52	70.6	0.93	hii
53001-1499-452	0.004	18.2597	0.972991	17.0	0.38	6.02	0.87	hii	53001-1499-525	0.003	18.4185	0.877542	20.2	0.41	8.74	0.76	non
53001-1499-527	0.003	18.5847	0.916690	18.8	0.36	63.3	0.99	non	53001-1499-577	0.065	18.7107	0.803241	19.0	0.31	11.5	0.94	hii
53001-1499-596	0.043	18.8711	0.703726	18.8	0.42	21.8	0.95	hii	53052-1562-056	0.037	44.6053	-1.07781	19.1	0.49	7.19	0.89	hii
53172-1031-596	0.204	328.742	0.574362	19.6	0.42	6.37	0.94	non	53175-1032-536	0.204	329.905	0.997784	19.5	0.39	5.94	0.86	non
53239-1025-120	0.050	317.415	-0.35844	18.5	0.35	15.2	0.99	hii	53239-1025-513	0.050	316.929	0.343028	17.5	0.44	10.1	0.96	non
53239-1025-531	0.187	317.069	0.855431	19.4	0.44	4.35	0.78	hii	53271-1558-221	0.042	35.1198	-0.43119	18.7	0.35	20.2	0.99	non
53271-1558-487	0.160	35.8396	0.570051	19.2	0.43	11.7	0.99	hii	53287-1555-270	0.059	29.0265	-0.00753	18.5	0.30	6.66	0.97	hii
53287-1555-276	0.358	28.8100	0.104836	19.7	0.32	12.4	0.98	non	53317-1560-056	0.176	40.3656	-0.75473	18.7	0.30	4.65	0.80	non
53730-1500-120	0.088	20.2711	-0.21799	19.2	0.41	11.0	0.76	hii	53730-1500-245	0.108	19.4387	-1.17558	19.7	0.35	5.52	0.88	hii
53730-1500-579	0.007	20.5374	0.948195	15.7	0.62	86.5	0.99	hii	53734-1542-472	0.106	5.11576	0.300462	18.6	0.44	3.09	0.91	hii
53740-1501-360	0.007	20.5515	0.948310	18.1	0.61	49.1	0.98	hii	53740-1501-412	0.016	21.4156	0.127994	19.4	0.42	26.1	0.95	hii
53740-1501-455	0.006	21.5197	0.315263	17.4	0.60	67.4	0.99	non	53740-1556-123	0.075	31.7642	-1.13393	18.8	0.50	3.16	0.86	non
53740-1556-188	0.042	31.4155	-0.68968	20.1	0.51	28.2	0.98	hii	53741-1502-510	0.026	23.5799	1.236970	19.1	0.43	20.2	0.93	hii
53742-1512-479	0.041	43.7070	0.039400	20.7	0.32	14.9	0.92	hii									



**Figure 1.** Examples of the spectral decomposition by the SSP method. In each panel, the observed SDSS spectrum (thin line), the best fitted results (thick line), the stellar components, the AGN continuum (dashed line) and the line spectrum are shown (from top to bottom). In order to show more clearer plots, each component has been smoothed using 8 nearest data points. The title of each panel shows the information of the SDSS MJD-PLATE-FIBERID for the spectrum.

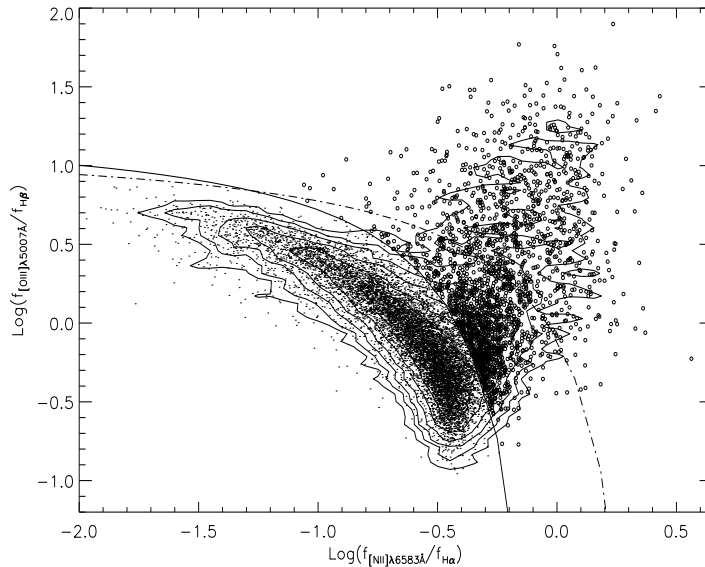


**Figure 2.** The BPT diagram for the pure narrow line objects. The solid line (the dot-dashed line) represents the dividing line between the AGNs (Seyferts and LINERs) and the HII regions discussed in Kauffmann et al. (2003) and in Kewley et al. (2009). The dots and the circles are the classified HII regions and the AGNs. The contour is created by the selected pure narrow line objects.

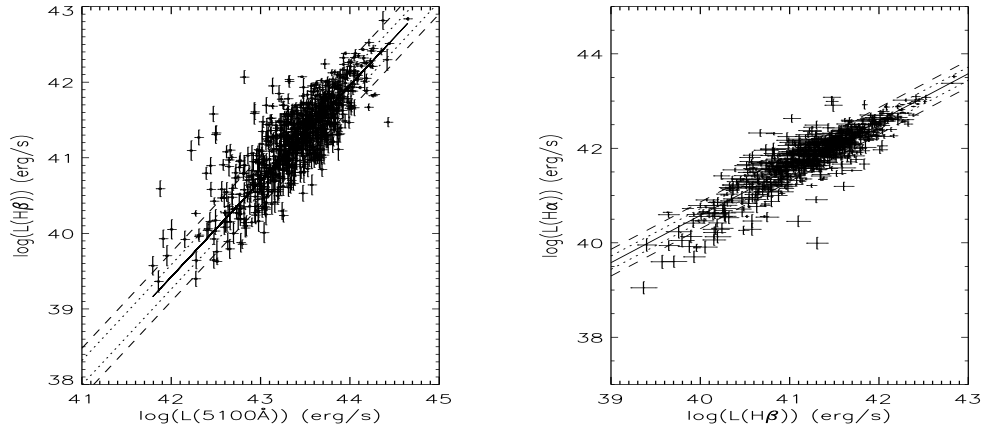


**Figure 3.** Correlation between the AGN continuum luminosity at 5100Å and the broad H $\beta$  luminosity (left panel) and the luminosity correlation between the broad Balmer lines (right panel), for the pure broad line AGNs. The solid line shows the best fitted result, the dotted line and the dashed line represent the 0.1dex and 0.2dex scatters for the corresponding best fitted result.

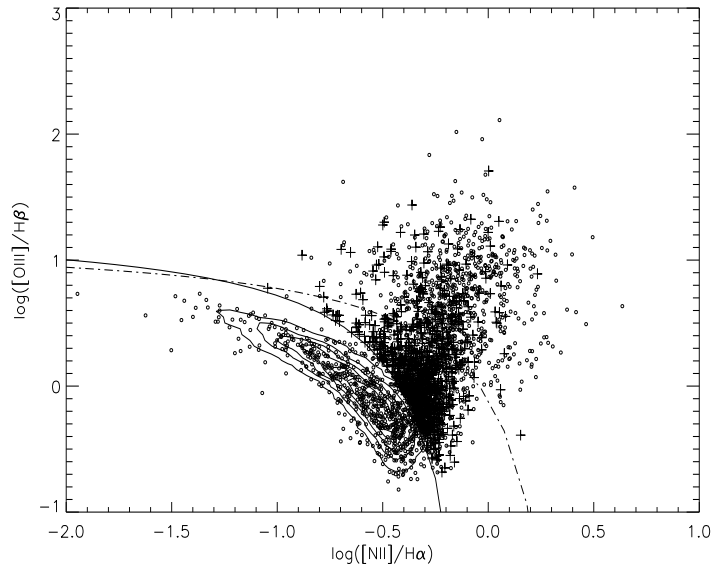


**Figure 4.** The BPT diagram for the broad line AGNs (including the pure QSOs). The contour located below the dividing lines represent the positions for the classified HII regions from the pure narrow line objects, the plus symbol represents the classified AGNs from the pure narrow line objects, the circles are for the broad line AGNs.

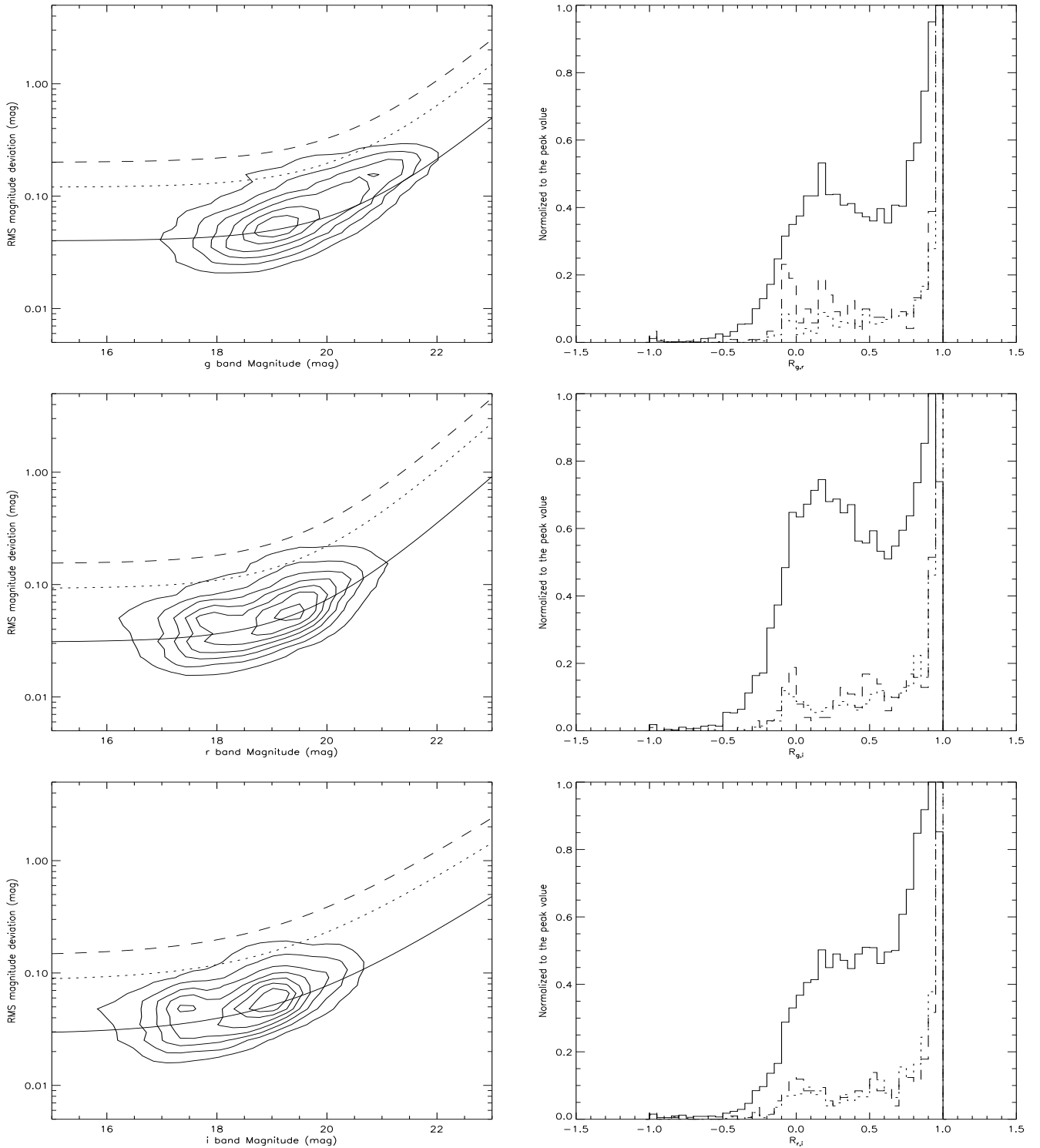


**Figure 5.** Properties of the RMS functions (left panels) and the Pearson's coefficients between two different band light curves (right panels) for all the galaxies and QSOs in the Stripe82 region. In the left panel, the contour (the correlation between the RMS deviation and the magnitude) shows all the objects (9254 QSOs and 51614 galaxies for the g band results, 9826 QSOs and 55795 galaxies for the r band results, 9728 QSOs and 54695 galaxies for the i band results), the solid line, the dotted line and the dashed line shows  $RMS_k/RMS_{M_k} = 1, 3, 5$  ( $RMS_k/RMS_{M_k} = 1$  means the results shown in the Equation (4)) respectively. In the right panel, the solid line, the dotted line and the dashed line represent the properties of the Pearson's coefficients for the objects with  $RMS_k/RMS_{M_k} > 1$  and for the objects with  $RMS_k/RMS_{M_k} > 3$  and for the objects with  $RMS_k/RMS_{M_k} > 5$  respectively.

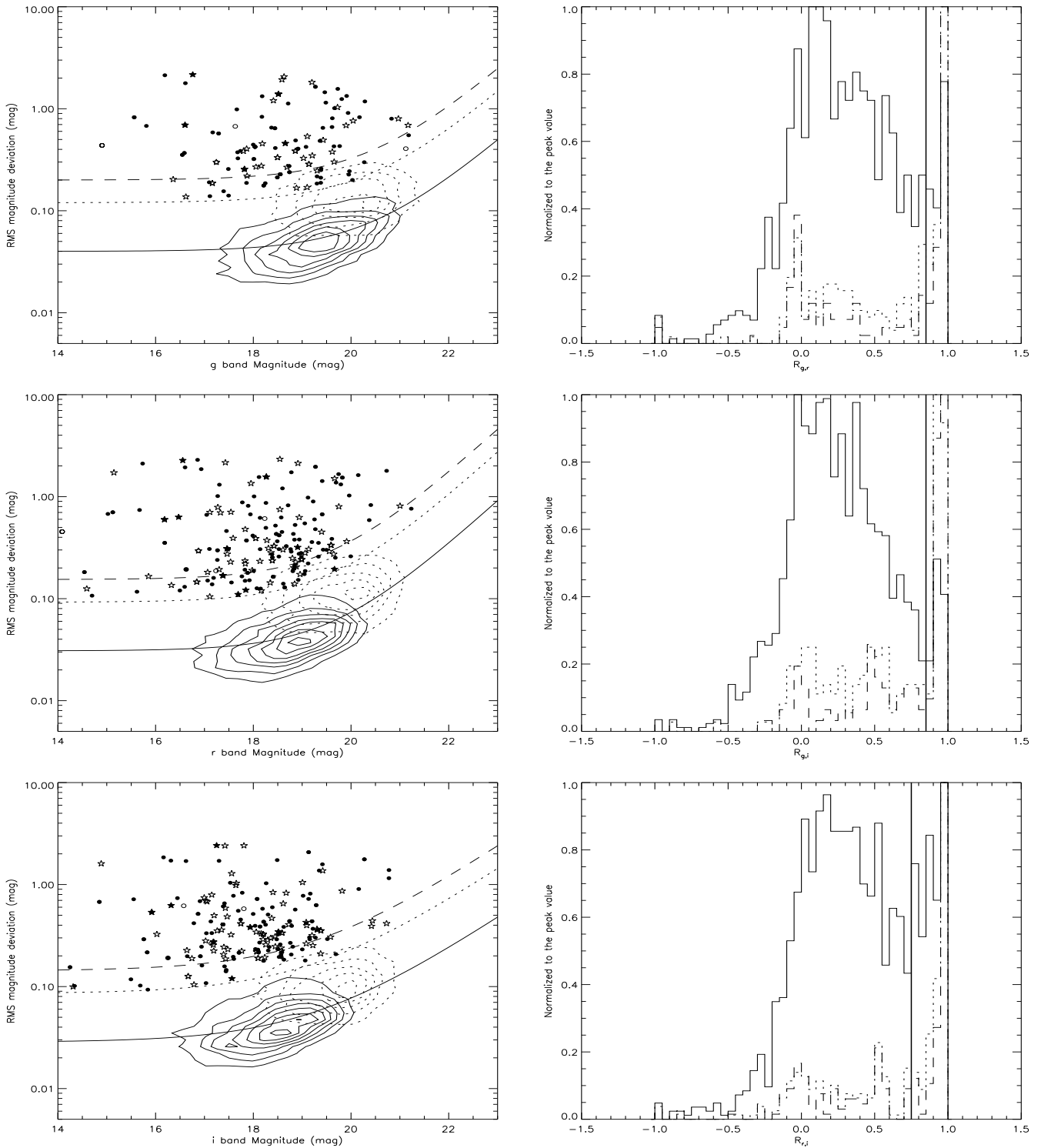


**Figure 6.** Similar as the results in Figure 5, but for the objects in our spectroscopic sample. And furthermore, in the left panels, the contour in solid line shows the properties of the narrow line objects in our spectroscopic sample, the contour in dotted line shows the properties of the QSOs in Stripe82 region. And in the left panels, all the 281 reliable candidates are shown with open circles (AGNs), solid circles (HII galaxies) and triangles (non-classified objects). In the right panels, the thick solid lines show the positions for the critical value of  $R_{1,2}$ .

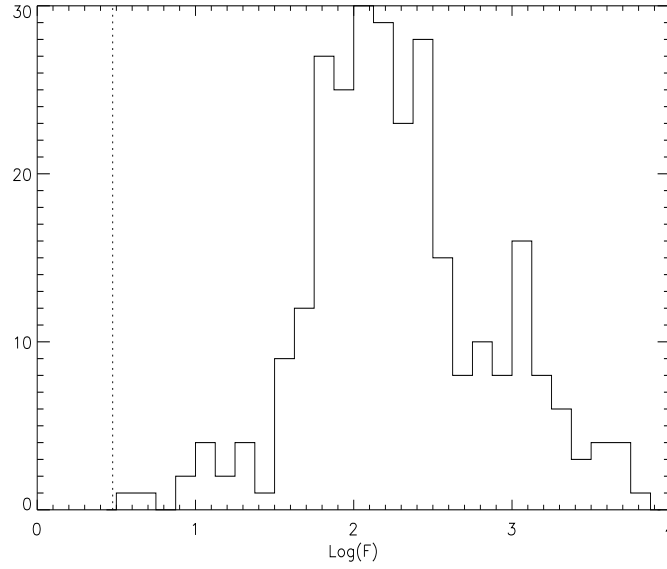


**Figure 7.** The F-test results. The solid line is for the distribution for the calculated F values by the Equation (7), the vertical dotted line is the F-value calculated by the F distribution.

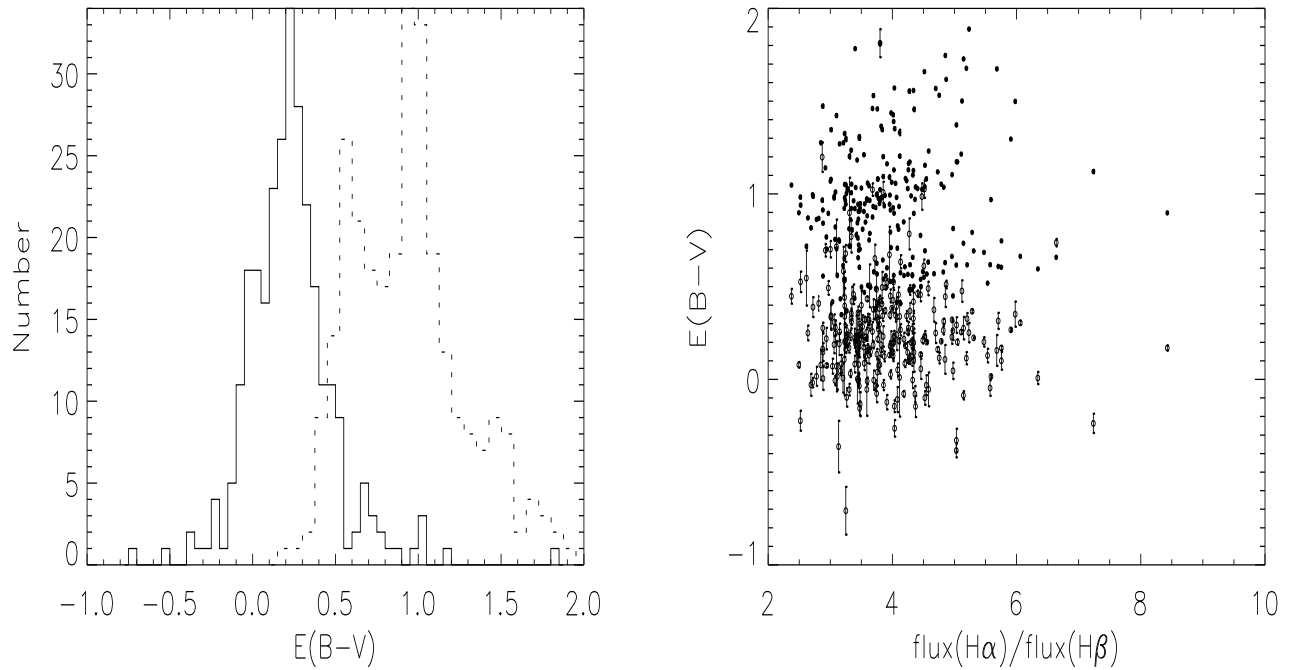


**Figure 8.** The properties of the dust extinctions with and without the considerations of the AGN continuum component  $P_{AGN,r_\lambda}$  for the 281 reliable candidates for the BLR-less AGNs. In the left panel, the solid line is for the results with the consideration of  $P_{AGN,r_\lambda}$ , the dotted line is for the results without the consideration of  $P_{AGN,r_\lambda}$ . In the right panel, it is shown the correlation between the flux ratio of the narrow H $\alpha$  to the narrow H $\beta$  and the parameter E(B-V). In the right panel, open circles are for the results with the consideration of  $P_{AGN,r_\lambda}$ , solid circles are for the results without the consideration of  $P_{AGN,r_\lambda}$ .

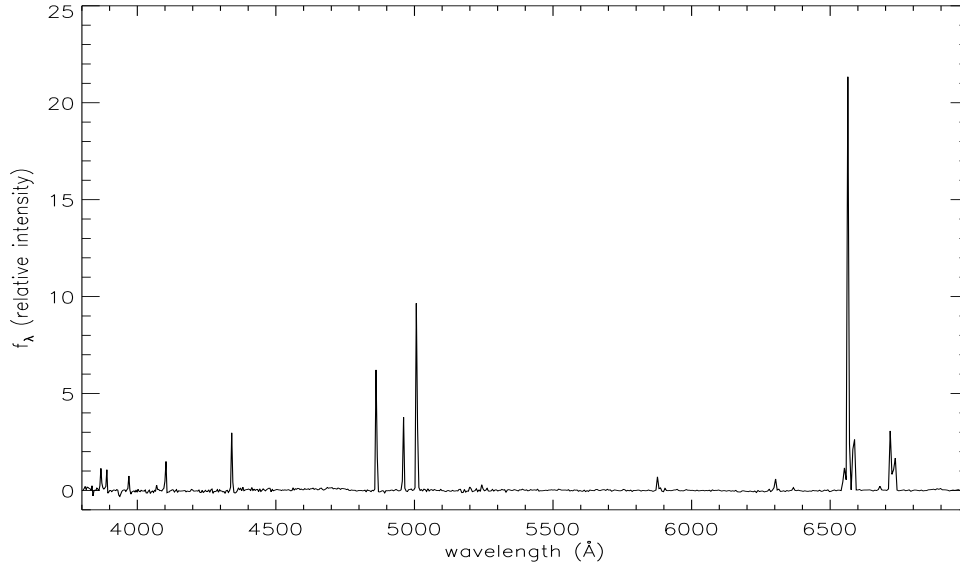


**Figure 9.** The mean spectrum of the 281 reliable candidates for the BLR-less AGNs, with AGN continuum components and the stellar components having been subtracted.

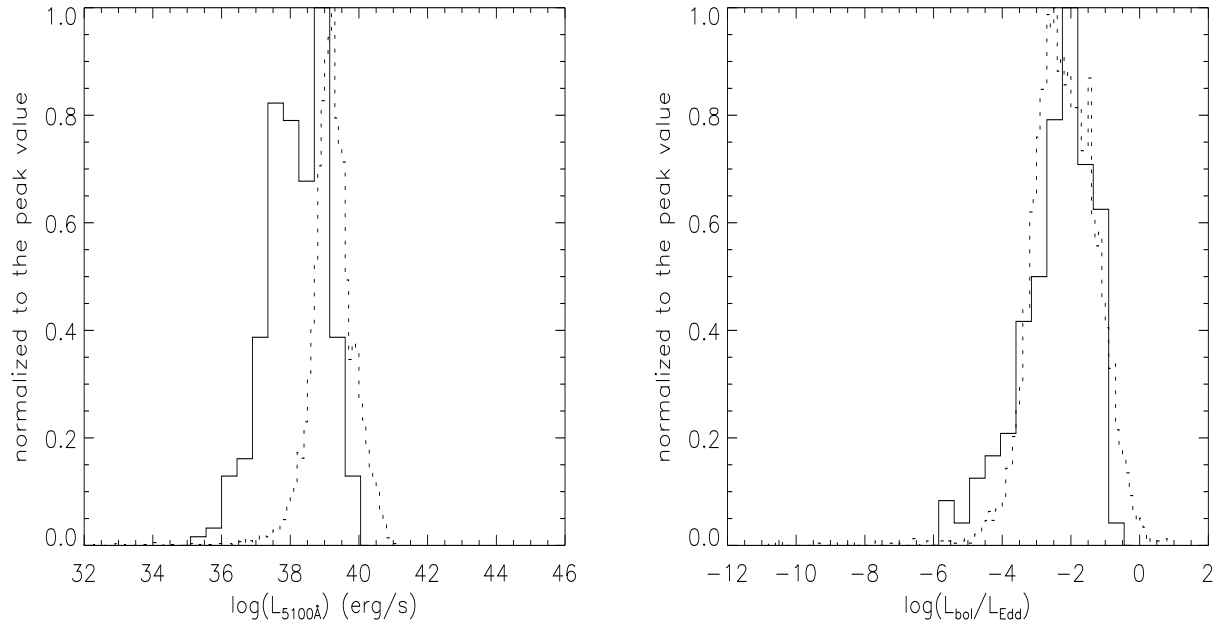


**Figure 10.** The properties of the continuum luminosity and the Eddington accretion rate for the reliable candidates for the BLR-less AGNs. The solid lines are for the BLR-less AGNs, the dotted lines are for the normal broad line AGNs.